arXiv:astro-ph/0107186v1 10 Jul 2001

Ultraviolet Spectrophotometry of Variable Early-Type Be and B stars Derived from High-Resolution IUE Data

Myron A. Smith[1]

[1]STScI/CSC, Space Telescope Science Institute, 3700 San Martin Dr. Baltimore, MD 21218 and Catholic University of America, Washington, D.C.; Email: msmith@stsci.edu

Received _____; accepted _____

ABSTRACT

High-dispersion *IUE* data encode significant information about aggregate line absorptions that cannot be conveniently extracted from individual stellar spectra. Herein we apply a new technique in which fluxes from each echelle order of a short-wavelength *IUE* spectrum are binned together to construct low-resolution spectra of a rapidly varying B or Be star. The division of binned spectra obtained during a "bright-star" phase by spectra from a "faint-star" phase leads to a ratioed spectrum which contains information about the mechanism responsible for a star's variability. The most likely candidate mechanisms are either the periodic or episodic occultations of the star by ejected matter or a change in photospheric structure, e.g. from pulsation. We model the variations caused by these mechanism by means of model atmosphere and absorbing-slab codes. Line absorptions strength changes are rather sensitive to physical conditions in circumstellar shells and "clouds" at temperatures of 8,000–13,000 K, which is the regime expected for circumstellar structures of early B stars.

To demonstrate proofs of concept, we construct spectral ratios for circumstellar structures associated with flux variability in various Be stars: (1) Vela X-1 has a bow-shock wind trailing its neutron star companion; at successive phases and hence in different sectors, the wind exhibits spectrophotometric signatures of a 13,000 K or 26,000 K medium, (2) 88 Her undergoes episodic "outbursts" during which its UV flux fades, followed a year later by a dimming at visible wavelengths as well; the ratioed spectrum indicates the "phase lag" is a result of a nearly gray opacity that dominates all wavelengths as the shell expands from the star and cools, permitting the absorptions in the visible to "catch up" to those in the UV, and (3) ζ Tau and 60 Cyg exhibit periodic

spectrum and flux changes, which match model absorptions for occulting clouds but are actually most easily seen from selective variations of various resonance lines. In addition, ratioed UV spectra of radial and large-amplitude nonradial pulsating stars show unique spectrophotometric signatures which can be simulated with model atmospheres. An analysis of ratioed spectra obtained for a representative sample of 18 classical Be stars known to have rapid periodic flux variations indicates that 13 of them have ratioed spectra which are relatively featureless or have signatures of pulsation. Ratioed spectra of three others in the sample exhibit signatures that are consistent with the presence of co-rotating clouds.

Subject headings: stars: Be – stars: circumstellar matter – stars: pulsation

1. Introduction

The cause or causes of the rapid light and spectrum variability of the "classical Be stars"[1] is a longstanding problem with no convincing universal solution at hand (see Baade & Balona 1994, Balona 1995, Smith 1999, Balona 2000, Baade, 2000). Both radial and nonradial pulsations (hereafter, "NRP") are endemic to this region of the H-R Diagram, but the physical attributes and manifestations of short- and long-period modes can be quite different. In many respects the latter modes are not well understood. Likewise, generally indirect evidence has been advanced that magnetic dissipation processes are somehow responsible for this rapid activity, even though magnetic fields have not been directly detected in nearly all Be stars examined. An indicator of magnetically-triggered expulsions of matter leading to Be "outbursts" could be the presence of magnetospheric structures similar to the co-rotating tori over He-rich Bp stars (Shore & Brown 1990). These tori (herein "clouds") absorb stellar flux as they occult the stellar disk and produce variability in broad-band UV light curves. If the structures are optically thick they can also produce variations in spectral line profiles of a rotating star that are similar in appearance to those produced by NRP. A broad consensus has formed (e.g., Smith 2000b, Baade 2000) that either or both mechanisms can play a role in ejecting mass from the surfaces of these stars, but even if both of them are operative their relative roles are unclear. To establish these roles requires that the mechanism for the variability be correctly assigned. Except for a relative handful of multiple-periodic Be stars, determining the variability mechanism is not always straightforward. Statistical studies (e.g., Balona 1990) suggest that the dominant periods of monoperiodic Be stars in visible-band light are consistent with the

[1]Classical Be stars as defined herein are post-zero age main sequence, non-interacting-binary B stars for which the Balmer lines have been observed in emission. This emission is generally as evidence of sporadic ejections of mass which form a flattened circumstellar disk.

stars' rotational periods, although the latter quantities are generally not well known. On the other hand, the variability periods are also in agreement with the range expected for long-period NRPs arising from g-modes.

In this paper we pose the question of whether candidate physical causes of the variability, most likely magnetospheric clouds or pulsations, can be determined in a Be star which is variable on a rotational timescale (see also Smith 2000a). In phrasing this question, we make the assumption that circumstellar clouds should be *cooler* than the line forming region of the nearby photosphere and thus should cause preferential absorptions among low-excitation metallic lines as they pass between the star and the observer. We will address this issue by introducing a spectrophotometric technique tailored to high-resolution, far-ultraviolet echellograms of the *International Ultraviolet Explorer* (*IUE*) satellite processed by *NEWSIPS* software.[2] This technique proceeds by binning all fluxes within each of 60 echelle orders to form an equivalent low-resolution spectrum. We then ratio this spectrum with another spectrum observed at a time when the flux of the star is different, that is, by dividing spectra from a "bright-star" phase(s) with those from a "faint-star" phase(s). The ratioed spectra so formed contain residual signatures of the variability mechanism because of the increased absorptions of an intervening medium or, in the case of pulsation because the temperature distribution or velocities in the photosphere are expected to be modified during a pulsation cycle. The resulting ratioed spectra are simulated by dividing a synthesized photospheric spectrum into a spectrum computed with absorptions from a slab of material in the line of sight.

Recently, Smith & Groote (2001) applied this spectrophotometric technique to evaluate physical conditions (temperature, turbulence, area, and column density) in magnetic torus-shaped clouds forced into corotation over two magnetic B stars, σ Ori E

[2]NEW Spectral Imaging Processing System (see Garhart et al. 1997).

and β Cep. They found that the weak metallic lines which are the principal absorbers in the far-UV are formed in column densities of about 10^{23} particles cm^{-2} and temperatures of 11,500–13,000 K. Because absorptions of metallic lines and continuous absorptions of hydrogen and H^- generally increase with decreasing temperature, these authors pointed out that spectrophotometric detections technique are most sensitive to low cloud temperatures (8,000–10,000 K). However, there are other ways to infer the existence of a warmer material in an intervening medium. Smith & Groote found that the principal UV resonance lines of spectra of these stars are very strong, suggesting that the clouds must also have a warm component. As previous investigators found before them, Smith & Groote reported that the UV profiles from the clouds associated with He-strong Bp stars maintain their shapes and strengths at a given phase over at least several years. In this paper, we ask whether putative clouds associated with Be stars could have these same general properties.

2. Reduction and Analysis of Archival IUE Data

2.1. Data Reduction

The *IUE* echellogram data for this study were the high-dispersion spectral files from the Short Wavelength Prime (SWP) camera. The echellograms were downloaded from the MAST[3] data archive. In most cases, and wherever possible, large-aperture observations were used. The data selected for comparison were obtained generally observations made within a day of one another, typically in an intensive monitoring program. These data selections essentially avoid errors due to long-term degradations in the camera as well as changes in the reference point in the aperture used to recenter the stellar image. One exception to our selection practice is for a proof-of-concept demonstration which we make below for 88 Her,

[3]Multi-Mission Archive at Space Telescope Science Institute, in contract to NASA.

the variations of which occur usually over a timescale of years. In separate work we have found that *NEWSIPS* calibrations are imperfect. For example, incomplete corrections in the *NEWSIPS* calibrations result in a residual systematic flux error of -1% yr^{-1} at most *SWP*-camera wavelengths; this correction is somewhat larger for wavelengths below λ1250 (Smith 1999a). These dependences can cause slowly varying time-dependent errors in the derived background fluxes of high-dispersion spectra, with resulting errors in the zero-point of the flux scale which affect net spectra at short wavelengths. Fortunately, these effects are generally unimportant over short timescales covered in intensive monitoring campaigns such as those we utilized principally in this study. In addition, ratios of spectral fluxes tend to be insensitive to such errors. Despite these grounds for optimism, an important part of our data conditioning procedure was the monitoring of the depths of highly saturated resonance lines such as the C IV and Si IV doublets, Lyman α, and Si III at λ1206 and λ1298. Because these lines are already completely saturated in the cores, the core depths cannot vary for astrophysical reasons, such as changes in atmospheric temperature or the added absorptions from circumstellar material. For spectra taken close together in time, the core depths of these lines remained constant to within $\pm$2% of the continuum level for nearly all the exposures in any one group. Thus, we adopted this value as the uncertainty of the background levels in the program spectra. For wavelengths above λ1500 these errors drop to about half this value.

Our numerical analysis of our data proceeded by means of a computer program which first loops through all echelle spectra for a given star and tabulates the core depths of saturated lines mentioned above. Attributing fluctuations of these depths to variations in the background level, we interpolated the implied zero-point offsets for orders between the resonance lines and extended them to these factors for short and long wavelength echelle

orders. Our code then computes corrections to the net fluxes[4] by applying the (nearly unitary) ratios of the average core depths for all spectra to the core depths of each individual spectrum. The code next sums all valid fluxes in each order (that is, it omits pixels with bad data quality flags) and creates a low-resolution spectrum from them. This process was repeated for each spectrum in a time series, producing a stacked array of low-resolution, high signal-to-noise spectral ratios. The effective resolution of the binned spectrum is given by the echelle's free spectral range, which is typically about 20 Angstroms.

The final phase of the data manipulation consists of computing a pseudo-measure of the ultraviolet continuum (hereafter, "UVC"), which is the average of the summed fluxes of four orders extending over the range $\lambda\lambda$1800–1905. We then relied upon a variability timescale, which is a period determined from ground-based or UV studies and is usually obvious in our *IUE*-derived flux curves as well. High-resolution spectra obtained at times when the star was UVC-bright were binned, co-added, and divided by the sum of spectra when the UVC flux was faint. This manipulation permits the computation of the ratio:

$$F_{obs}(\lambda) = 1 - f_{min}(\lambda)/f_{max}(\lambda) \ . \tag{1}$$

We will use the term "ratioed spectrum" as short-hand in this paper to refer to this equation. Depending on the astrophysical mechanism causing the variability, this spectrophotometric ratio can be related either to a theoretical ratio of two photospheric spectra or to one minus the occulted spectrum to the unocculted photospheric spectrum.

[4]Herein we treat exclusively net fluxes rather than "absolute calibrated" fluxes in order to avoid unnecessary spectrum-to-spectrum errors in the ripple-correction process. The net fluxes of an echelle order provide a natural wavelength bin unit because they rise from low values at one end of the order and drop to low values again at the other end.

Errors in the ratioed spectra depend on several factors. One of the most important of these is the loss of sensitivity at short wavelengths. Both Smith, Robinson, & Hatzes (1998) and Smith & Groote (2001) determined r.m.s. errors of ±0.8% at long wavelengths which increased to ±1.5% at short wavelengths using binned flux-ratioing of *IUE* data. We have examined the r.m.s. fluctuations of a few ostensibly nonvariable stars and found values averaging ±1.1% for wavelengths above λ1300. These estimates are based on both internal (point-to-point) variations and comparisons of ratioed spectra from data obtained from different groups of observations. For this study we have relied on two new approaches to address systematic errors, which we describe as follows.

In the first approach, we selected a pair of echellograms for the B3Ve star α Eri. These observations (SWP 55873 and SWP 55889) were obtained 0.7 days apart, which is about half the principal 1.26 day variability cycle discovered by Balona, Engelbrecht, & Marang (1987; see also Leister et al. 2000). We constructed a ratioed spectrum both from *NEWSIPS*- and *IUESIPS*-processed data. The background flux solutions derived by these processing systems are altogether different. Although the *NEWSIPS*-derived values are usually more accurate (but typically slightly low), they were derived by sampling non-local as well as local fluxes on the echellogram. In contrast, *IUESIPS* backgrounds were determined only from local fluxes and tend to be high. Figure 1 shows spectral ratios from both extractions. We take their differences to be a generous estimate of errors resulting from flux extractions. Note that both curves start near unity at long wavelengths and increase almost monotonically toward short wavelengths. A "spike" at Lyman α in the ratioed spectrum resulting from the fluxes of both constituent spectra being low and hence producing an uncertain ratio. At long wavelengths the mean ratios of the *IUESIPS* and *NEWSIPS* spectra are nearly identical, and the difference between them is typically ±1.5%. At shorter wavelengths these errors increase until at λ1160 the curves become meaningless. The important result here is that the curves are mutually consistent, suggesting that the

low-resolution spectral ratios are insensitive to the method of flux extraction.

To evaluate the effects of background flux errors, we repeated our manipulation of the same pair of *NEWSIPS* spectra, but this time we lowered the background by an assumed error which is linear in decreasing wavelength and normalized it to -2% of full continuum at 1250 Angstroms. The dashed curve in Fig. 1 exhibits the result of dividing this modified spectrum by the original one – that is, the result of the perturbed background flux levels. This curve again increases toward shorter wavelength and also causes a faint spike at Lyman α. In all, although the amplitude of these features is small, the spectrum-to-spectrum deviations in background level can potentially could produce second-order errors at short wavelengths.

As a second approach to evaluating systematics in ratioed spectra, we constructed an artificial "knife-edge test" by comparing pairs of spectra of a nonvariable star. In one case one spectrum was obtained with the star within the aperture, and in the other case it had begun to drift to the aperture edge. We selected two pairs of small aperture spectra for this purpose for the stars 16 Lac and η Ori (SWP 05858 & 05860 and SWP 22163 & 22158). These observations were obtained during times when the stars appeared otherwise constant in brightness. Inverting the ratios to represent an artificial brightening, we found that the ratioed spectra exhibited slopes of -20% and -2% with respect to their mean flux ratios minus one. Thus, this is a nearly flat but slightly red response. Both ratioed spectra showed r.m.s. fluctuations of about 1%, which is consistent with the r.m.s. values quoted above.

2.2. Computation of Simulated Spectra and Spectral Absorptions

To model the observed spectral ratios, we used a suite of codes written by I. Hubeny and collaborators to compute synthesized ratios of stellar spectra (in the case of pulsation)

or absorptions of the stellar spectrum (in the case of an occulting medium). To mimic our actions on the observed data, we first divided the spectra one by the other and then binned them to the effective free spectral range of the *SWP* camera. For the case of pulsation, in which one photospheric spectrum is divided by another, the comparison to the observations is conceptually straightforward because computed and observed ratios are nearly unity. For the case of absorbing clouds the computed absorptions are normalized to the stellar continuum. Then, a weak absorption spectrum ratio will be some fraction between zero and one.

The first of the Hubeny codes, *SYNSPEC*, is a spectral line synthesis program developed for input non-LTE and/or line-blanketed model atmospheres (Hubeny, Lanz, & Jeffery 1994). We used standard LTE model atmospheres by Kurucz (1993) as input to *SYNSPEC*. *SYNSPEC* is embedded within an IDL wrapper (Hubeny 1996) to facilitate the calculation of spectra for a variety of atmospheric parameters. For our program we ran models with log g = 4, a microturbulence of 5 km s^{-1}, and no rotational broadening. Another available option in *SYNSPEC* is to modify the run of atmospheric temperature, T(ρx). We used this option to mimic variations in the temperature gradient which occur during a radial pulsation.

To simulate the effects of a cloud on the composite spectrum, we used the Hubeny *CIRCUS* program (Hubeny 1996, Hubeny & Heap 1996). This code was written to compute line absorptions and/or emissions of a gas cloud situated either in front or off the limb of a reference star. These absorptions comprise the so-called "iron curtain" in the ultraviolet. *CIRCUS* requires the user to specify physical cloud parameters such as temperature, density, geometry, composition, microturbulence, column depth, and areal coverage factor. The computations are performed at the same wavelengths as for the synthesized photospheric spectrum. *CIRCUS* can accommodate clouds with as many as three separate sets of

conditions, sizes, and positions. However, in this work we considered mainly homogeneous clouds. In its solution of the radiative transfer equation *CIRCUS* computes line emission and absorptions separately. These options can be treated as "switches" and permits the investigator to evaluate the two effects separately. The cloud temperatures we consider are generally less than 20,000 K. For this temperature range reemission in both the resonance transitions and weak iron-curtain lines is negligible.

CIRCUS proceeds by consulting a Kurucz (1990) line library of atomic absorption parameters and computing an opacity spectrum for a user-specified temperature, composition (solar), and electron density. The spectra were computed at a spacing of 0.01 Angstroms, thereby resolving most UV lines in the Kurucz line library. The optical depth in each line is determined from the computed opacity spectrum and the input column density. The surface of the star is divided into a grid and the local intensity spectrum is evaluated at each grid point, thereby taking into account effects of foreshortening and limb darkening.

The density and geometrical coverage factors of the assumed cloud are additional necessary parameters in our analysis. For our initial models we started with a trial volume density of 10^{12} cm^{-3}. This estimate is based on the probable cloud densities of 10^{11}–10^{12} cm^{-3} that appear to prevail in the rotating magnetic B stars (e.g. Smith & Groote 2001). For simplicity we ran models with a full (100%) areal coverage factor. The actual coverage factor for any given case may be obtained by scaling the full-coverage models to the observed level of the ratioed spectra (minus one). The positions and amplitudes of individual absorption peaks in the observed spectral ratio can then be used to determine the cloud temperature and column density, respectively.

CIRCUS includes a provision for various doppler effects, including stellar rotation. The program computes the net doppler velocity between each projected element of the cloud and the background star along the observer's line of sight. For a co-rotating cloud

the velocities along the line of sight are the same, so the net shift is zero. Another relevant factor in determining cloud absorptions is the microturbulence. However, Smith & Groote (2001) found that velocities less than 20 km s^{-1} produce similar cloud spectra, so we used this value as a default.

3. Results for General Models

3.1. Homogeneous Clouds

Over a broad range of possible cloud temperatures, the density of metallic metallic lines increases with decreasing temperature in nearly all ultraviolet and visible band regions. For a reference cloud model of $T_{cloud} \approx 13{,}000$ K and a particle density $N_H = 3{\times}10^{-12}$ cm^{-3}, the sum of the hydrogen bound-free absorption and electron scattering coefficients is about $8{\times}10^{-25}$ cm^2. For this model we tabulated the number of local maxima in computed absorption spectrum and found a total of some 26,000 unblended lines. The median strength of these lines is only 65% as strong as the continuous opacity, so the majority of the lines becomes optically thick at almost the same column density as the underlying opacity continuum. In the optically thin limit the wavelength binning of the absorption spectrum to $\sim$20Å generates amorphous "features" due to local line aggregates which can arise above the continuous absorption by a factor of up to 2–3. A detailed inspection of the line strength distribution in the $\lambda\lambda$1150–2000 wavelength region shows that the median strength is typically higher than the lower-envelope of the absorptions by only tens of percent. Thus, except in the case of strong lines (Lyman α, resonance lines of Si III, Si IV, and C IV), the binned spectrophotometric features are nearly as optically thin as the absorption windows between them. This fact explains why the calculated spectra are insensitive to the microturbulence velocity parameter ξ_t over a range of values. For intermediate column densities the optically thin features diminish in amplitude and gradually lose their identities.

As one increases the column still further, the absorptions finally become optically thick at all wavelengths. For cloud temperatures of 8,000 K and 13,000 K, this happens for column densities of about 1.5×10^{23} and 3×10^{24} cm^{-2}, respectively. At this point the fraction of absorbed flux increases to about 80% to 90%, respectively, and the spectrum shape becomes almost flat.

Although the morphology of the absorption spectrum depends on the contrast with the underlying photospheric spectra, our *CIRCUS* models suggest that the detailed features are well preserved over a typical range in effective temperatures of ±3000 K for $T_{eff} >$ 13,000 K. Figure 2 exhibits absorption spectra computed for a variety of indicated cloud temperatures, a column density of 1×10^{23} cm^{-2}, $N_H = 3\times10^{11}$ cm^{-3}, $\xi_t = 20$ km s^{-1}, and coverage factor of 1. Because the postulated clouds co-rotate with the star, the results are the same for nonrotating and rotating star inputs. We have also run models of rapidly rotating stars and with intervening clouds having no doppler component along the line of sight, i.e., the case of quasi-static *shells.* The primary departures from the co-rotating cloud models are that resonance lines exhibit slightly added absorptions because their saturations are lifted by the velocity difference along the line of sight.

Changes in cloud temperature greatly modify the shape of the ratioed spectrum, particularly for values less than 11,000 K. This is a combined result of the increased hydrogenic absorption and a shift from third to second-ionization stages of chiefly the Fe-group elements. Consider especially how cool temperatures affect strong lines: the most prominent feature arises from the resonance Si III line at 1206 Å and Lyman α, which dominate two adjacent wavelength bins. Other sharp features in the binned ratioed spectrum are caused by resonance lines of Si IV (≈λ1400) and C IV (≈λ1548-50), and from excited multiplets of C III (λ1176) and Si III (≈ λ1300). All of these features are visible for temperatures ≥ 13,000 K.

Resonance lines are less visible for cool temperatures ($T_{cloud} < 11{,}000$ K). This is partly a consequence of the continuous opacity becoming stronger as hydrogen recombines. In addition, as these lines disappear resonance lines of second-stage ions appear at longer wavelengths, often beyond the *SWP* camera range. However, a few resonance lines of less ionized species still play roles in the general rise of absorption for all cloud temperatures considered, particularly at wavelengths below λ1200. A good example is the confluence of Si II $\lambda\lambda$1190–1197 lines which fall near a number of strong excited Fe III lines. In addition, at lower temperatures the Si II lines saturate and form strong damping wings. These increased absorptions, along with the still-strong Si III λ1206 and Lyman α lines form a strong composite absorption. When these features are binned with a group of nearby excited Si III and low-excitation Fe II lines, they produce a general increase in absorption below Lyman α.

At longer wavelengths several broad features form that provide convenient diagnostics of temperatures in ratioed *SWP* spectra. The most well known of these is the absorption centered at λ1900 (e.g., Bjorkman, Bjorkman, & Wood 2000; hereafter "BBW"). This broad feature appears at a clouds temperatures between 10,000-17,000 K and attains its maximum strength at 15,000 K. The absorption is largely due to a variety of excited (χ = 8–10 eV) Fe III lines. For temperatures less than about 9,000 K the ionization of iron shifts from Fe^{2+} to Fe^{1+}, causing an important Fe II absorption feature to appear at $\lambda\lambda$1600–1700. A secondary peak at λ1850 is formed at cool temperatures largely from excited Fe II atoms. An additional weak peak centered near λ2050 is formed from an assorted collection of excited second-ionization lines of iron-like atoms and Fe I resonance lines. Recently, Groote & Smith (2001) were able to use weak features near λ1650 and λ1900 in the binned spectral ratios of the magnetic B stars σ Ori E and β Cep to determine temperatures in the outer regions of their co-rotating clouds.

3.2. Nonradial and Radial Pulsations

Nonradial pulsations on a star cause different regions to move both horizontally and vertically, causing periodic modulations in atmospheric temperature and pressure. An external observer viewing this activity will alternately view a dominance of first hot and then cool regions as the pattern moves across the projected stellar disk. By ratioing atmospheric fluxes from these regions, one obtains a spectrophotometric signature of the pulsations. In Figure 3a we exhibit this behavior to first order by ratioing the synthesized spectra of static atmospheres having effective temperatures of 26,000 K and 22,000 K. This example clearly represents an exaggeration of flux variations in most NRP stars, but it serves to emphasize the signatures of a simple atmospheric flux ratio. Even so, the only clear temperature signatures are weak flux-ratio elevations corresponding to the Lyman α line and the Si III λ1300 multiplet. Unlike the cloud absorption models, this ratioed spectrum displays no "sharp" feature at $\lambda\lambda$1100–1150. Small-amplitude fluctuations at long wavelengths are the result of an incomplete cancellation of a complex array of line strengths in the two constitutent spectra. Otherwise, this ratio may be roughly characterized as a monotonic function increasing with decreasing wavelength. Other authors (e.g., Peters 1991, Cugier, Daszynska, & Polubek 1996, Peters 1998b) have exploited this dependence by fitting UV variations of NRP early-B stars to *IUE SWP* spectra.

As the terms suggest, radial pulsations differ from nonradial pulsations in that the locally imposed motions are vertical. As such, they are coherent over the entire stellar disk at any given phase. The local velocity amplitudes of the radial modes in a few β Cephei stars can be very large, even exceeding the atmospheric sound velocity. Such motions typically modify the atmospheric structure by enhancing the temperature difference between the line and continuum formation regions. Occasionally, sharp absorption features appear at low negative velocities and then move redward through the line profile as a consequence

of pulsational shock waves traveling through these atmospheres (e.g., Campos & Smith 1981, Smith 1983, Mathias, Gillet & Crowe 1992). Phase delays are well known to occur for resonance lines formed in superficial atmospheric layers (e.g., Burger, de Jager, & van den Oord 1982). We have pursued the Burger et al. finding by inspecting line fluxes of a number of strong lines in the spectra of the large-amplitude pulsators BW Vul and ν Eri during their radial pulsation cycles. All the lines we investigated showed a pronounced strengthening as the pulsation wave entered the line forming region. Atmospheric simulations show that two ways of simulating these strengthenings is to lower the atmospheric boundary temperature (or in the more realistic formulation of non-LTE, one accounts for lowered excitation temperatures of lines due to the radiation boundary) or to increase the velocity broadening (e.g., microturbulence) of the spectral lines. The temperature effect also can be inferred in the reddening of the colors of β Cep stars during the phase of maximum distension (relative to phase of compression). Although dynamic model atmospheres do not exist for β Cep stars, we have utilized these facts to make a simplified approximation in creating a pair of modified model atmospheres by altering the temperature distribution T(ρ x) for a T_{eff} = 24,000 K, log g = 4 Kurucz atmosphere to mimic the effects of the passing wave in strengthening the "temperature" gradient. The temperatures in the line formation regions (ρ x = 10^{-3}–10^{-2}) of these models differ from the reference atmosphere by $\pm$400 K, which is a typical temperature amplitude in the atmosphere of a β Cep star over the course of a pulsational cycle. These distributions are displayed in Figure 3b. We also increased the atmospheric microturbulence from zero to 15 km s^{-1} in the steep-gradient model in order to attempt to simulate the effects of turbulence following the passage of a shock wave (Stamford & Watson 1981). Synthesized spectra were then generated from these altered models and ratioed. The result is displayed in Fig. 3c. One can see from this that the results of perturbing the atmospheric distribution cause appreciable differences in the aggregate absorptions of spectral lines and therefore in the appearance of the two

photospheric spectra. Thus, the ratioed spectra resulting from these simple descriptions of radial and nonradial pulsations (Fig. 3a) are quite different. Notice that flux contrasts at Lyman α again produce a local spike in the ratioed spectrum. However, a broad feature appearing at $\lambda\lambda$1240–1375 has a more subtle explanation. The lines in this spectral region are comparatively sparse except for several strong Si III and C II lines near λ1300. The latter region is also nestled between the strong line Si III λ1206 and Ly α lines on one side and many stronger lines above λ1375. These lines respond sensitively to the steepening of the temperature gradient. Highly saturated lines in the spectrum, such as λ1206, are sensitive to increases in microturbulence. The overall effect of this arrangement of strong lines is to create the illusion of a transparent window at $\lambda\lambda$1240–1380 punctuated by a sharp peak at λ1300. A weak "plateau" is often also present in the region between the Si IV and C IV doublets, and this is due to a large assortment of Fe-group lines. Two weak absorption features at λ1650 and λ2000 have similar explanations.

We emphasize that the particular atmospheric model described above in the radial pulsation simulation is simplistic and probably a nonunique. Furenlid et al. (1987) have suggested that line variations in BW Vul may be due in part to a decrease in the atmospheric continuous opacity. We tested this possibility by comparing synthesized spectra obtained from 24,000 K models having $\log g = 4.5$ and 3 with the same microturbulences as before. We found that the ratioed spectra from these spectra show the same general spectrophotometric features as those shown in the Fig. 3c. Thus, we conclude that the described spectral features are robust attributes which are produced by modifying the atmosphere in such a way as to strengthen the formation of most lines, as is indeed observed in *IUE* spectra.

4. Analysis

4.1. Proofs of Concept: Intervening Slabs and Clouds

In this section we discuss in detail four variable B stars for which independent evidence exists that circumstellar gas sometimes occults the star. All but the first of these examples are well-observed classical Be stars which are probably observed, respectively, through an expanding shell, a density wake, or rapidly appearing and disappearing structure which could be a magnetosphere.[5] In each case, the ratioed spectrum displayed a pattern of spectrophotometric signatures which can be fit with *CIRCUS* models. These demonstrations show both the power and limitations to determinations of physical conditions of circumstellar matter from UV spectrophotometry.

4.1.1. Vela X-1 = HD 77581 = 4U 0900-40

Vela X-1 is a high-mass X-ray binary composed of a B0.5 Ib primary and a X-ray pulsar in a close, nearly-circular orbit. Because the components are close ($a \approx 1.6$ R$_*$, P = 8.96

[5]For additional comparison to the Be stars, we also examined three interacting Be binaries for which the UV resonance lines are known to show strong emission variations with phase (e.g., Peters & Polidan 1984). Assuming several observations were present, these stars' spectra could not have be confused with those of Be stars or magnetic rotating B stars for several reasons. The continuuum fluxes show either negligible variations (e.g., CX Dra, HR 2142) or variations so large that they must be caused by an eclipse of one stellar component (e.g., AU Mon). The resonance emission lines of these systems span a large range across the profile, including their blue wings, and are often morphologically distinct from one ion to another. A filling in of the C IV and Mg II profiles at some phases, which results from emission in a large volume of gas around the mass-receiving star, is not seen in spectra of the Be or magnetic B stars.

days) and the orbit is almost aligned to our line of sight ($i > 74^o$; van Kerwijk et al. 1995), the neutron star transits the primary every orbital cycle. The wind from the B star accretes onto a surface surrounding the pulsar, permitting a detailed mapping of a complex wind environment. In the conventional picture (e.g., Kaper et al. 1993) wind particles emanating from the supergiant in this system form an accretion shock which trails the orbiting pulsar. This shock radiates at X-ray energies, resulting in the ionization of an X-ray Stromgren sphere out to some distance. Because ultraviolet radiation is largely transparent in this region, the accelerating force on the B-star wind particles nearly vanishes as they enter the Stromgren sphere, leaving them free to coast across the sphere at velocities they acquired before entering this region. As the particles leave the trailing edge of this sphere, they interact strongly with high velocity particles whose accelerations have not been interrupted. This interaction creates a second, spiral-shaped "photoionization wake" which runs from a point near the B-star's surface outward and behind the neutron star (Blondin et al. 1990). In these models the shocked region cools with distance from the Stromgren sphere, so material cools as one moves outward along the wake. The wake intersects the line of sight to the B star for perhaps a whole cycle, so one expects to observe the cooled wake in UV resonance lines at phases much later than the transit of the pulsar (at $\phi = 0.5$) and indeed just before the next transit. Kaper et al. (1993, 1994) have argued that Vela X-1 is a case where these complex interactions are readily observable. They point in particular to line profile asymmetries in a number of optical and ultraviolet resonance lines if one compares them from phases just *after* ($0.5 < \phi \leq 0.6$) transit compared to just *before* ($0.4 \leq \phi \leq 0.5$) this event. These authors noticed that low-velocity features present at other orbital phases vanish at phases just after a transit and attributed this to the absence of wind material to an ionization change in the wind as it enters the photoionization wake. By contrast, the accretion wake surrounding the pulsar is not likely to be responsible for this variability because it is very small and also because it is too hot to absorb UV line flux.

To investigate the prediction of Kaper et al., we have formed ultraviolet quasi-continuum light curves from orders corresponding to $\lambda\lambda$1800–1905 from all 50 available *SWP* large-aperture spectra. We corrected the fluxes for the 1978 epochs by -7% to bring their values into agreement with late-epoch spectra; this correction is consistent with the -1% yr^{-1} noted above for degradation of long-term far-UV *IUE* fluxes. The resulting light curve, displayed in Figure 4a, shows a slightly asymmetric ≈10% dip at phases 0.46–0.70 centered at $\phi \approx 0.52$. Close inspection of the behavior of these absorptions reveals a different wavelength dependence just before and after light minimum. To make this point quantitatively, we have divided spectra during the first ($0.40 < \phi < 0.46$) and second ($0.5 < \phi \leq 0.60$) halves of the pulsar transit by four spectra observed at phases prior to the pulsar transit (ϕ = 0.28–0.30). These spectra have the highest continuum fluxes (Fig. 4a) and are presumed to be least affected by the effects of a photoionization wake. These ratios (minus one) are shown as Figure 4b and c. The ratioed spectrum in Fig. 4b exhibits long-wavelength absorptions, including a clear Fe III absorption bump at λ1900. As discussed in §3.1, this feature suggests a cloud temperature in the range 11,000–17000 K. For phases just before transit, the ratioed spectrum in Fig. 4b can be reproduced quite well with a model having T_{cloud} = 13,000 K, and a column density of $1\times\ 10^{23}$ cm^{-2}, all scaled to a coverage of ≈60%. (For this model we used assumed parameters of T_{eff} = 25,000 K, log g = 2 for the computed underlying photospheric spectrum; see van Kerkwijk et al. 1995). In contrast, the ratioed spectrum shown in Fig. 4c for post-transit phases is dominated by a broad hump at λ1550. This broad feature is not replicated by our moderate or cool-temperature models (cf. Fig. 2). However, models run with considerably higher temperatures show that the feature is due to many aggregates of Fe III and IV lines. Our best-fitting match to the ratioed spectrum was with a model with T_{cloud} = 26,000 K. The absence of strong absorption features (other than from the C IV doublet) at this temperature suggests a large column density, so we used a value of 3×10^{23} cm^{-2}.

At this column density the absorption is large, and this must be compensated to fit the observations by a relatively small coverage factor of 28%. We should also point out that the sharp dip in the observed spectral ratios at λ1400 (Si IV) is not necessarily a detriment to our shock-wake model. This feature is actually a *reflex* of warm wind material viewed at $\phi = 0.3$.[6] Overall, Fig. 4b is typical of the absorption spectrum one might expect from a moderately dense wind from an early-type B supergiant. In contrast, Fig. 4c suggests the presence of a local hot slab with a higher column density. Finally, we remark that extracted He λ1640 line strengths from these spectra (not shown) exhibit a clear increased absorption of this line lasting $\approx$0.35 cycles centered at $\phi = 0.5$. This is the transit phase of the neutron star and indicates the presence of a hot source along this line of sight. Putting this all together, these models argue for a wind the properties of which vary substantially with azimuthal position in the orbital plane. This is a good working description of the photoionization wake suggested by Kaper et al.

4.1.2. 88 Herculis = HD 162732

88 Her is a late B-type classical B star (T_{eff} = 15,000 K; Harmanec 2000) which has undergone a series of long "outbursts" over at least the last few decades. We define an outburst here by the appearances of Balmer and metallic "shell" lines accompanied by a decrease in continuum flux at UV and visible wavelengths (Harmanec et al. 1978, Doazan et al. 1982). It is generally believed that an outburst corresponds to the ejection of an initially opaque envelope which becomes optically thin as it slowly expands over many stellar radii and cools. Be stars like 88 Her typically decline in brightness at first and then

[6]Judging from the P Cyg profiles of the Al III doublet at all phases, warm material is present in all lines of sight around the orbital cycle.

gradually return to their pre-outburst levels. As the outburst cycle proceeds, the near- and far- ultraviolet spectra acquire low-excitation "shell" absorption lines of Fe III Fe II, Ni II, and similar ions (Danezis & Theodossiou 1988, 1990). During 1976–1978 the UV brightness of 88 Her faded by about one-third and by 1979 had reattained its previous flux (Barylak & Doazan 1986). The visible-band flux faded as well, but its decline lagged by about by about a year behind the UVC curve. In their compendium study of *UBV* light curves of Be stars, Pavlovski et al. (1997) showed that the visible flux of 88 Her had nearly recovered to its former maximum by the early 1980's, only to fade once again in the mid-1980's. As with the previous cycle, the V-band fluxes lagged a year behind the U and B fluxes.

The archival high-dispersion *IUE* spectra cover the period 1981–92. The beginning of this interval coincided with a stabilization of the flux from the previous outburst. Detailed examination of the *IUE* spectra shows that strong Fe III lines were present during this entire period, including the beginning of the outburst. Figure 5a exhibits the UVC light curve ($\lambda\lambda$1800–1905); again, a +1% yr^{-1} correction has been applied to the fluxes. The decreases in the flux show that another extinction episode occurring during the early 1980's. By 1987–8 the UV brightness had decreased by 40% and then brightened again during 1990–1992, virtually recovering to its initial maximum.

We computed spectral ratios systematically as a function of epoch during the mid- and late-1980's by using three spectra obtained near 1982.0 to represent the most unobscured state. The ratios depart appreciably from unity only after 1985 when the absorptions exceeded 10%. In Figure 5b we display the ratioed spectrum formed from spectra obtained in 1982.0 and 1986.0–.4. As one proceeds to the larger spectral ratios formed from 1987–8 data, corresponding to observations taken during the UVC minimum, the ratioed spectra become flatter and almost devoid of features. In principle, these could be easily confused with ratioed spectra of Be stars without intervening matter (e.g., see Fig. 9), except that

they show a hint of increased absorption near λ1650 and λ1900. More importantly, they also show selective variations of resonance line strengths of Al III, Si III, and Fe III, a fact that demonstrates that cool material along the line of sight must be present at some times. A periodogram of the UVC light curve from one month to several years exhibits no peaks that might be present from gas streams between members of an interacting companion of long period. In particular, when folded over the 86.6-day orbital period suggested by Harmanec, Koubsky, & Krpata (1974), the UVC fluxes show no correlation with phase. Thus, the UVC and line variations are not likely to be caused by binary interactions.

Upon investigating constituent pairs of spectra in pre- and post-outburst groupings, we found that the various ratioed spectra we formed were self-consistent and fit the ratioed spectrum with a *CIRCUS* model having a low temperature and a fairly high column density. The best fits resulted with models with cool temperatures ($\approx$ 8,000 K) and high column densities. For these values, H^- continuum opacity effectively dominates even the near-ultraviolet, so the morphology of the absorptions is flatter than the lower column density models depicted in Fig.2. Figure 5b shows two fits to these for the necesssarily high column densities of 3×10^{23} and 6×10^{23} cm^{-2}. To obtain these fits we used coverage factors of 35% and 28% respectively. Since one might expect that a nearly optically thick cloud should be extensive, and thus should occult the star completely, we attempted to find models with 100% coverage factors. However, we were unable to push coverage factors much higher (and the column densities lower) without producing substantially more prominent absorption features than are present in the data. Nonetheless, we believe that the fit to the observed features is quite good for wavelengths above $\sim\lambda$1250.

Because the opacity increases with decreasing temperature, the absorptions of hot gas embedded in a cool cloud can easily be concealed in the binned spectral ratios. Of course, this statement does not necessarily hold true for individual lines in a high-dispersion

spectrum. In fact, an investigation of the Fe III line behavior also disclosed evidence for the presence of warmer gas along the line of sight than the 8,000 K component determined from the weak iron-curtain lines. This evidence takes two forms. First, low-excitation lines of Fe III (and Al III) show occasional variations on a timescale of a few months. These variations do not correlate with the features in the UVC light curve in Fig. 5a. Second, the variations of these lines are largest among moderate-excitation lines (≈ 10 eV). Fig. 5c shows a comparison of spectra in the λ1910 region obtained both in the UVC-minimum and recovery periods (i.e., at 1987.5 and 1990-2). Variations in the strengths of these lines are obvious. Absorptions for models with $T_{cloud} \geq 13{,}000$ K can easily produce changes in moderate-excitation lines, but low-excitation lines are too saturated already for the dense (or extensive) clouds to have much effect on them.

According to the time histories of the Fe III line strengths, warm intervening gas was present present along the path to 88 Her during its entire outburst cycle during the 1980's. The amount of this gas varied at times over intervals as short as a few months, perhaps as a result of fresh ejections of material. These additions cause the column length to vary by $\sim 3 \times 10^{22}$ cm^{-2} over intervals short compared to the total outburst cycle. From this evidence, rapid injections of warm gas seem to have expanded outward from the star and cooled during the long outburst cycle. Such a picture leads naturally to an understanding of the time lag of the visible flux after the UV minimum in 88 Her during a typical cycle: initially the ejected plasma is warm and absorbs mainly in the far-UV. As the gas cools, the opacity becomes grayer, so the absorption of flux absorbs nearly equally at near-UV and visible wavelengths. Consequently, the visible-band flux falls to nearly the same level as the UV flux, creating an apparent lag in visible-band light curve. Note also that in this interpretation there appears to be no need to postulate a change in effective temperature of 88 Her during the outburst, as suggested by Doazan et al. (1986) and discussed further by Smith (2000b). These authors were led to this interpretation based on observations showing

that the star faded and brightened simultaneously over the λλ1550–5500 region. However, we suspect that the redistribution of absorbed light would have become apparent as a flux *brightening* in the near-infrared if the observations could have been extended to this region as well.

4.1.3. ζ Tauri = HD 37202

ζ Tau is a well-known B2e star with an extensive flattened circumstellar disk which has been imaged using optical interferometric techniques (Quirrenbach et al. 1998). Making use of two absorption bumps at λ1900 and λ2400, BBW recently fit scattering models to UV spectropolarimetric (*WUPPE*) data to a temperature of 14,000 K for the inner disk. ζ Tau also exhibits variable line profiles of Hα and He I λ6678 over a 0.78-day period. Kaye & Gies (1998) initially attributed this periodicity to nonradial pulsations. However, Balona & Kaye (1999) later reinterpreted the profile variations in terms of two co-rotating clouds, one at a low and the other at a high stellar latitude. In the first paper, Kaye & Gies speculated that sharp occasional absorptions in line profiles are formed in orbiting cloudlets over the star. Thus, the presence of close circumstellar material (in addition to the star's circumstellar disk) seems to have been accepted by both groups of authors.

Figure 6a shows that the ≈0.8 day period is well defined in the UVC curve. Using the two pairs of observations indicated in the caption, we computed the spectral ratios and computed the mean in spectrum in Figure 6b. The r.m.s. errors are taken from the two constituent ratioed spectra. In computing this mean, we found an offset of 1% between these curves, either because of instrumental reasons or because the absorptions had actually changed. For presentation in our figure we have corrected the respective scales of the two ratioed spectra by -0.5% and +0.5% in order to refer them to a common mean. Except below λ1250, the two binned spectra agree quite well. In approaching the simulation of

these observations, we were guided by the especially prominent variations of the Al III λ1855–63 doublet (see Fig. 6c), since the local maximum near λ1900 in Fig. 6b is subtle at best. These lines indicate the presence of cool circumstellar matter. Using an effective temperature of 21,000 K for ζ Tau, (BBW, Harmanec 2000), a best fit to the line strength variations gave a a cloud temperature of 8,000 K ($\pm 2,000$K), a column density of 2×10^{23} cm^{-2}, and a coverage factor of 20% to fit the ratioed spectrum. Except for the lower column density, this is essentially the model that we used in Fig. 5b for 88 Her. We should add that the spectrum of this model shows a mean absorption level for wavelengths above λ2000 that is $\sim$20% higher than is observed. A similar small disparity occurs for 88 Her in this narrow wavelength region. This difference could be due to errors in atomic parameters or (in our view, less likely) to an error in the flux linearization of *NEWSIPS* at these wavelengths. Despite this discreprancy, the quality of the fit of the model is good and thus lends support to the Balona & Kaye interpretation of a magnetic co-rotating cloud over this particular star.

Turning our attention to the behavior of prominent spectral lines, we note the report by Kaye and Gies (1998) that the He I λ6678 line of ζ Tau can vary in strength by 0.5–1% of the continuum over several hours. Simulations of this line with *CIRCUS* show that such variations can be reproduced in clouds over a wide range of cloud temperatures. To determine a lower temperature limit for the He I line variations, we ran models to see what temperature ranges could just produce additional absorptions of 0.5%. We found the lower limit to the temperature to be 11,000 K. Perhaps not coincidentally, this is also the value for which λ6678 becomes optically thick in a spherical cloud with the dimensions determined from the 20% coverage factor. Because the absorptions from a warm cloud component could be hidden in the model shown in Figure 6c, the appearance of He I line variations does not contradict the spectrophotometrically derived value of 8,000 K. Another indication of the presence of a torus-cloud is variability in the Fe III "resonance" line spectrum near

λ1910 (not shown). This variability is detectable in lines with lower levels up to 6 eV, but not much higher, and is consistent with absorptions from a warmer gas than suggested from the Al III and iron-curtain lines. To simulate these variations, we ran several *CIRCUS* models for temperatures of 8000–15,000 K with column densities similar to those required in our models of the He I λ6678 line. With cloud temperatures in the 10,000–12,000 K range, our models well reproduced the Fe III variations. Thus, both the Fe III and He I line variations support a second, warm (>10,000 K) cloud component, in addition to the cooler one inferred from the Fe-curtain lines. As with the case of 88 Her, a warm secondary cloud component could easily be hidden in a multi-temperature model of the spectrophotometric absorptions.

A few additional comments should be made about the circumstellar body indicated by the variations in the curtain and Fe III resonance lines. The first is that a trade-off between the coverage factor and the column density is possible in the fit to the Fig. 6b spectrum. We find that larger coverage factors and higher column densities cause features in the ratioed spectrum to increase and decrease, respectively. The coverage factor may be thought of merely as a scaling parameter, so as it decreases any spectrophotometric details will tend to decrease in visibility. A higher column density makes the variation smaller too because at this temperature the effects of foreground absorption are more nearly gray. For these reasons we cannot rule out a model with a higher column density of, say, 5×10^{23} cm^{-2} and a coverage factor of 13%. Our preference for the fit depicted in Fig. 6b was constrained from the recognition that variations of the resonance lines, such as the Al III lines depicted in Fig. 6c, would be difficult to explain with models invoking inordinately high column densities and an attendant saturation of the strong metallic lines. Both the resonance lines of Al III and the Fe III lines near λ1910 require model column densities of 10^{22--23} cm^{-2}, depending on the assumed temperature, to match the observations. In addition to a cloud width-length trade-off, we found that the contrast of the λ1900 and neighboring bumps in

the ratioed spectrum can be simulated with multi-temperature cloud models, but with a clear loss of uniqueness.

Thirdly, it is conceivable that the variations of both the He I and Fe III lines could instead arise from a 0.78-day NRP modulation in the photosphere. However, to this hypothetical suggestion, one can respond that there is additional evidence that the Fe III lines in these observations vary on long timescales and thus are often unrelated to conditions near the surface. In investigating the behavior of the Fe III lines, we found that there are considerable differences between the line strengths in 1991 and additional observations some four years later. Moreover, by 1995 the star's UVC flux had brightened by 10–15%, whereas the strengths of all Fe III and Al III lines became much weaker. The simplest explanation for these changes is that the column length of material in front of the star had decreased in this time. We suspect that this condition arose from changes in the circumstellar disk rather than the smaller, co-rotating clouds we have considered in this work. Changes in the column density of the disk would not necessarily mean that the disk structure had changed during this time. Indeed, it could also have changed its orientation. The disk of ζ Tau is thought to be non-axisymmetric in density and to precess around the star with a period variously estimated to be 2.3 or 7 years (Delplace 1970, Vakili et al. 1998). Hence, long-term changes in the column length of circumstellar material could be due to disk precession.

4.1.4. 60 Cygni = HD 200310

60 Cyg is a B1Ve star which exhibits light variability with a 2.48 day period (Harmanec et al. 1986). Figure 7a depicts the UVC light curve for this star taken from *IUE* *SWP*-camera observations in July, 1995. This curve appears consistent with this period, but there appear to be variations on other timescales as well. Koubsky et al. (2000) have come

to a similar conclusion from visible-wavelength data. These authors also note that the star has a mild helium enhancement, which hints already that the star could have a co-rotating magnetosphere. An inspection of *IUE* spectra reveals that the star's spectrum shows a very strong N V doublet as well as variable emission in both this and the C IV doublets. These are indeed signatures are co-rotating clouds associated with rotating magnetic B-stars (Smith & Groote 2001). We next grouped the *IUE* spectra into bright- and faint-star star phases according to this period. An example of this comparison is displayed in Figure 7b. This ratioed-spectrum plot shows a weak but discernible absorption bump at λ1900. This feature, along with the overall, nearly flat, shape of the absorption spectrum, can be used to set constrain the temperature of the co-rotating cloud inferred from the presence of variable resonance lines discussed in the following paragraph. In general, the same comments about the geometrical and temperature trade-offs discussed for ζ Tau (Fig. 6b) apply to the fit of Fig. 7b, but to a lesser extent. We also exhibit our best fit in Fig. 7b, based on these trade-offs and a *CIRCUS* model with T_{eff} = 26,000 K and cloud parameters T_{cloud} = 13,000 K, column density = 1×10^{23} cm^{-2}, and a coverage factor of 60%.

Figure 7c exhibits typical spectral variations of the Al III and a nearby Fe II line. Other high excitation lines in the *SWP* spectra, such as He II λ1640, show no detectable variations, indicating that a medium cooler than the photosphere is responsible for the low-excitation line activity. Modeling of the variations of these three lines shows probably fortuitously good agreement with the parameters obtained from panel (b). The average of the 3 line variations shown in panel (b) is 18 $\pm$3%, and of the modeled variations, 21%. A "perfect match" to the mean of the variations of these lines could be made with T_{cloud} = 12,000 K. We estimate the actual errors on our fits from the spectral fitting are relatively large, about $\pm$2500 K, because of the large rotational broadening. In sum, the evidence from this figure supports an interpretation from the strong C IV and N IV lines of 60 Cyg (cf. Smith & Groote 2001) that most or all of its UV spectral variations are caused by

cloud occultations. However, if such clouds exist, the evidence from the light curve and the drifts of multiple subfeatures across the optical line profiles (Koubsky et al. 2000) suggests an ephemerality reminiscent of the clouds in γ Cas (Smith & Robinson 1999).

4.2. Pulsation

One of the first results to emerge from our study was that a distinct spectrophotometric pattern is present in binned ratioed spectra of radially pulsating β Cephei stars (§3.2). This result is depicted for six of these variables with known radial pulsation modes in Figure 8. These features are largest in stars having large pulsation amplitudes, such as BW Vul and ν Eri. A simulated ratioed spectrum (taken from Fig. 3b), is shown for reference. A comparison of the observations with the simulation shows strong similarities in the detailed absorption pattern. This fact suggests that they arise from an increased temperature gradient and/or microturbulence. Evidently, the ratioing of *SWP* spectra provides a new way of determining whether radial pulsations are responsible for a star's light and spectral variations.

We also discovered that a large-amplitude, *nonradially* pulsating star, ϵ Persei, exhibits a noticeable pulsation signature even though all its excited modes are nonradial (l = 3–5; Gies et al. 1999). The velocity amplitudes of the largest of these modes are very large and at times rival the atmospheric sound speed (Smith, Fullerton, & Percy 1987). Because the periods are short, the dominant velocities are directed nearly nearly vertically upwards or downwards at opposing phases. These pulsations also cause local temperature and pressure changes, which can cause a net change in the equivalent width of the line. Evidently, these effects do not completely cancel when integrated over the visible disk. In fact, line strength changes from these pulsations are visible in the ratioed spectrum of this star in Fig. 8 (bottom line).

We should point out that in our depiction of the pulsational signatures of β Cep (Fig.8) we obtained observations taken over just *one* pulsation cycle. Smith & Groote (2001) used ratioed spectra over different phases of this 12-day *rotation* cycle of this same star to demonstrate the presence of a co-rotating cloud. In the material used for constructing the β Cep curve in our figure, the cloud absorptions were equally present during both bright- and faint-star pulsation phases. Hence, the spectrophotometric ratioing technique can be utilized in a several-hour time series to detect pulsations in a magnetic star occulted by a cloud.

4.3. Application to Be Stars

The primary goal of our study was to see whether spectrophotometric information derived from short-wavelength *IUE* observations can be used as an tool for candidate variability models operating in Be stars such as nonradial pulsation and magnetic co-rotating clouds. One answer to this question is that the discrimination between the NPR and cloud models requires corroborative evidence, such as the selective strengthening of low-excitation lines on the timescale of the star's rotation period. Table 1 summarizes results for 18 early-to-mid Be stars with rapid and arguably periodic UV continuum variations. These are stars from a more complete sample of early-type Be stars assembled by the author which have been observed repeatedly by the *IUE* satellite during its lifetime.[7] "Group 1"

[7]Several stars in our original sample did not exhibit significant UV variations and are not represented in the table. These are 59 Cyg, θ CBr, X Per, 66 Oph, 48 Lib, and ζ Oph. The observations of several other demonstrable variable stars were too widely spaced in time for a reliable analysis. Marginal results were found for three stars, 28 CMa, κ CMa, and α Ara, and are discussed following the presentation of Table 1.

in the table consists of five stars, each of which shows at least mild ($\geq 8\%$) UV variations and for which ratioed spectra exhibit the pulsational signatures, discussed in §3.2 These are similar to those in Figs. 3 and 8. In Figure 9a we exhibit ratioed spectra of η Cen, DU Eri (HR 1423) EW Lac, λ Eri and which show these same signatures. The signatures are stable for these stars, being present consistently for different combinations of faint- and bright-phase spectra. If ϵ Per serves as a model, large-amplitude pulsations can produce strong, local atmospheric gradients in temperature and/or velocity which have signatures visible in far-UV spectra. From the length of the periods the pulsations must be nonradial pulsations.

Group 2 in the table consists eight Be stars with periodic UVC variations that are nearly monotonic with wavelength. Fig. 9b depicts ratioed spectra of 28 Cyg, o And, ϵ Cap, and ω Ori as examples. The spectrum for α Eri, also in this category, has already been shown in Fig. 1. The ratioed spectra of these stars do not show repeatable discrete features, but rather a tendency to rise toward short wavelengths. This pattern is consistent with the ratio of spectra synthesized from model atmospheres with different values of T_{eff} and is also in keeping with the (small-amplitude) nonradial pulsation paradigm in which spectrum contrasts are produced over time as mutually cancelling cool and hot regions travel across the disk with phase (Fig.1c). Of course, such an explanation does not rule out the alternative interpretation of absorbing clouds. However, the continua of the clouds' absorption spectrum would necessarily have to be optically thick and the coverage factors would have to be nearly 100%. In addition, we noticed in our data inspection that the resonance lines can have variable amplitudes from one brightness cycle to the next. Hence, if the variability of these stars arose from cloud absorptions, the clouds would have to be able to change their structures over a timescale of about a day. One cannot rule out the presence of large clouds with such transient properties, but this phenomenology is not present in clouds over rotating magnetic B and Bp stars. Thus, the spectrophotometric diagnostics

favor nonradial pulsation for most or all the stars in Group 2 arise from nonradial pulsation as well.

The spectrum of α Eri, previously displayed in Fig.1, is a case that should be singled out for special discussion. A direct comparison of its spectra and its UVC light curve reveals that the photospheric components of this star's Si IV and C IV resonance lines are *anticorrelated* with periodic UVC variations, and they probably have a small phase delay. Moreover, time series of optical spectra of this star disclose that the He I λ5876 and λ6678 lines can have variations which are not morphologically similar (Rivinius 1999). All these behaviors are puzzling according to our current understanding of nonradial pulsations. Nonetheless, other patterns, such as the variation of the Al III doublet, can be understood easily within the context of NRP. For example, these lines do not have deep cores that would be indicative of a cloud or shell at any phase. In addition, the wings of these lines strengthen during the "faint star" phase of a cycle. This fact can be explained simply as the result of an ionization shift occurring in a high density gas, i.e., at the high temperature extremum in a temperature-modulating photosphere. Hence this behavior argues for nonradial pulsations in α Eri.

Finally, Group 3 of Table 1 consists of three stars with cool co-rotating magnetospheres. We have already discussed the arguments for including 60 Cyg and ζ Tau in this group. In addition, we include the unusual Be star γ Cas. We do not discuss this star herein because we have treated it at length elsewhere (Smith, Robinson, & Hatzes 1998) and also because this star's X-ray and UV variability patterns are unique.[8]

[8]However, we can add here that variations of the C II λ1335–6 and Si II λ1200 lines show a clear correlation with the continuum light curve, as would be expected for clouds having a cool component.

Three other stars, 28 CMa, α Ara and κ CMa, which turned up in the course of our investigation are not listed in the table. However, they have redshifted emission in the Si IV and C IV lines and therefore are candidates for having torus-clouds. In the spectrum of 28 (ω) CMa one finds mild redshifted emission components in C IV and Si IV lines which vary on an unknown timescale. These characteristics could be explained in principle variable P Cygni-type wind activity, but probably not for the strong N V absorptions in the spectrum of this relatively cool (B2.5 IV-V) star. Optical work shows that 28 CMa is also an apparently-single star viewed at a nearly pole-on orientation in which the lines exhibit profile variations attributed to NRP (Maintz et al. 2000; but see Balona et al. 1999). In addition, optical lines formed at low densities and/or temperatures show their own special rapid, quasi-periodic behavior, suggesting the presence of a rarified structure above the photosphere (Stefl et al. 1998, Stefl et al. 2000). The *IUE* spectra of the rapidly rotating B2.5Vne star α Ara likewise exhibit redshifted emissions in the C IV and Si IV lines that are variable even over 2 hours. This star has neither a variable radial velocity history (Thackeray 1966) nor a high X-ray flux (Cohen, Cassinelli, & MacFarlane 1997) that could be indicate the presence of hot gas streams in an interactive binary. A third conceivable cloud-bearing candidate, κ CMa (B1.5IVne), was observed with the *IUE SWP* only three times, but its C IV and Si IV lines once again show weak redshifted activity and possible emission, though on an indeterminate timescale. N V absorptions are also visible. Balona (1990) has noted rapid photometric variations consistent with the rotational period during an outburst of this star.

4.4. Conclusions

This study has demonstrated that high-dispersion *IUE* archival spectra of variable B stars can be manipulated to bring out qualitatively new information about the mechanisms

responsible for these variations. Bjorkman, Bjorkman, & Wood (2000) have recently used UV spectrophotometry to determine physical attributes of circumstellar material around Be stars. In contrast to our technique, their study exploited the polarization signatures of asymmetrical *large-scale* circumstellar structures from single observations. Although our study has been limited to *IUE SWP* data, it also could be extended in principle to long-wavelength camera data of large-amplitude late-B, A-, and F-type variables.

In §4 we demonstrated how quantitative information can be gleened about gas ejected by hot stars. Our examples included Be stars which are surrounded by a compressed wind-wake, eject shells, have co-rotating clouds, or undergo large-amplitude pulsation. Indeed, our binned spectrum-ratio results demonstrate that quasi-monochromatic spectrophotometic changes of a Be star do not necessary imply the variation of its photospheric temperature from pulsation (cf. Peters 1998b), although this may well be the rule. The technique does not work well for determining parameters of inhomogeneous clouds or even of cool, dense clouds with small projected areas. Even so, we have seen that the presence of a warm cloud component may be inferred from a spectral analysis of specific lines in the same observations. Because residual errors in flux calibrations are still present, *IUE* data are limited in how they can be utilized over extended time periods. Still, they are useful in the some cases. For 88 Her in particular the progressive change in line strengths during an outburst shows that the "phase lag" of a dip in the *visible-band* light curve can be understood by the cooling of an expanding shell. Thus, the technique can compliment post-outburst observations of high-level Balmer lines and infrared emission studies in Be stars. It can be particularly helpful in quantifying changes of shell parameters with distance from the star.

Although one goal of this study was to diagnose the physical cause(s) of light and absorption line variability in classical Be stars, our success in using UV spectrophotometry

for this purpose must be said to be mixed: potential ambiguities could arise between dense clouds and weak NRPs in some cases. According to our "Group 3" list, Be stars with candidate co-rotating clouds actually show identifiable spectrophotometric signatures in only three of five cases. Even leaving aside such unique stars as γ Cas, a good case can be made for the existence of magnetic co-rotating clouds in only a minority of Be stars. Aside from the parenthesized entries our sample is relatively unbiased of variable early-to-mid B stars (as far as we know), so one may take the implied fraction of them having clouds to be about 1/8–1/4. These rough statistics suggest a magnetic cause (or trigger) for the Be phenomenon in at least a minority of classical Be stars. The existence of co-rotating clouds in particular seems to be a by-product of *dipolar* fields (Shore & Brown 1990) However, evidence exists also for *localized*, transient magnetic activity in other Be stars. Such evidence includes rapid line profile variability (e.g., "dimples"; Smith & Polidan 1993), and in the case of λ Eri, the appearance of an X-ray flare. Thus, it is possible that localized fields can play a role on the surfaces of other Be stars. Unfortunately, hypothetical prominence-type clouds associated with small-scale magnetic loops on Be stars (e.g., Peters 1998b) could not be detected with ratioed *IUE* spectra. Thus, we look to future optical studies of cloud-candidate Be stars to confirm the results of this work. Evidence of transits of low-density and temperature clouds might be found in high-quality time-series spectra, both in the appearance high-level Balmer lines and as occasional brief events observed in many lines.

We wish to acknowledge our appreciation to Dr. Ivan Hubeny for making his *SYNSPEC* and *CIRCUS* codes available to us. We also thank Dr. Dietrich Baade who made several comments that led to substantial improvements in this paper and also several helpful comments by the referee. This work was conducted in part under NASA NAG 5-8793.

REFERENCES

Baade, D. 2000, The Be Phenomenon in Early-Type Stars, op. cit., p. 178

Baade, D. & Balona, L. A., 1994 Pulsation, Rotation, & Mass Loss in Early-Type stars, eds. L. Balona, H. Henrichs, & J. Le Contel (Dordrecht: Kluwer), p. 311

Balona, L. A. 1990, MNRAS, 245, 92

Balona, L. A., 1995, MNRAS, 277, 1547

Balona, L. A. 1999, MNRAS, 306, 407

Balona, L. A. 2000, The Be Phenomenon in Early-Type Stars, *op. cit.*, p. 1

Balona, L. A., Engelbrecht, C. A., & Marang, F. 1987, MNRAS, 227, 123

Balona, L. A., Kaye, A. B. 1999, ApJ, 521, 407

Balona, L. A., Marang, F. et al. 1987, A. & A. S., 71, 24

Barylak, M., & Doazan, V. 1986, A. & A., 159, 65

Bjorkman, K. S., Bjorkman, J. E., & Wood, K. 2000, The Be Phenomenon in Early-Type Stars, ed. M. A. Smith, H. F. Henrichs, & J. Fabregat, ASP Conf. Ser. 214, p. 603 (BBW)

Blondin, J. M., Kallman, T. R., Fryxell, B. A., & Taam, R. E. 1990, ApJ, 356, 591

Burger, M., de Jager, C., & van den Oord, G. H. J. 1982, A. & A., 109, 289

Campos, A. J., & Smith, M. A. 1981, ApJ, 238, 250

Cohen, D. H., Cassinelli, J. P., & MacFarlane, J. J. 1997, ApJ, 487, 867

Cugier, H., Daszynska, J., & Polubek, G. 1998, Rotation, Pulsation, & Mass Loss in Early Type Stars, *op. cit.*, p. 17

Danezis, E., & Theodossiou, E. 1988, Ast. & Astrophys. Suppl., 72, 497

Danezis, E., & Theodossiou, E. 1990, Ap. & Sp. Sci., 72, 497

Delplace, A. M. 1997, A. & A., 7, 459

Doazan, V., Harmanec, P., et al. 1982, Astr. Ap. Sup., 50, 481

Doazan, V., Thomas, R. N., & Barylak, M. 1986, A. & A., 159, 75

Floquet, M., Hubert, A. M., et al. 1998, A. & A., 335, 565

Furenlid, I., Meylan, T., Young, A., Haag, C., Crinklaw, G. 1987, ApJ, 319, 264

Garhart, M. P., Smith, M. A., Levay, K. L, Thompson, R. W., & Turnrose, B. E. 1997, NEWSIPS Manual, IUE NASA Newsletter No. 57

Gies, D. R., Kambe, E. et al. 1999, ApJ, 525, 420

Harmanec, P. 2000, The Be Phenomenon in Early-Type Stars, *op cit.*, p. 13

Harmanec, P., Horn, J. et al. 1978, Bull. Astron. Inst. Czech., 31, 144

Harmanec, P., Horn, J., et al. 1986, IBVS No. 2912

Harmanec, P., Koubsky, P, & Krpata, J. 1974, A. & A., 33, 117

Hubeny, I. 1996, "Complete Guide to Generate Stellar Spectra under the Influence of Absorbing and/or Emitting Bodies," priv. comm.

Hubeny, I. & Heap, S. R. 1996, ApJ, 470, 1144

Hubeny, I., Lanz, T., and Jeffery, S. 1994, Newsletter on Analysis of Astronomical Spectra, 20, 30

Kaper, L., Hammerschlag-Hensberge, G., & van Loon, J. 1993, A. & A., 279, 485

Kaper, L., Hammerschlag-Hensberge, G., & Zuiderwijk, E. J. 1994, A. & A., 289, 846

Kaye, A. B., & Gies, D. R. 1998, ApJ, 482, 1028

Koubsky, P., Harmanec, H. et al. 2000, The Be Phenomenon in Early-Type Stars, *op cit.*, p. 280

Kurucz, R.L. 1990, Trans. IAU, 20B, 169

Kurucz, R. L. 1993, "ATLAS9 Stellar Atmospheres and 2 km s^{-1} Grids," Kurucz CD-ROM #13

Leister, N. V., Janot-Pacheco, E., Leyton, Z. J., Hubert, A. M., & Floquet, M. 2000, The Be Phenomenon in Early-Type Stars, op. cit., p. 272

Maintz, M., Rivinius, T., Tubbesing, S., Wolf, B., Stefl, S., & Baade, D. 2000, The Be Phenomenon in Early-Type Stars, op. cit., p. 244

Marlborough, J. M. 2000, The Be Phenomenon in Early-Type Stars, *op. cit.*, p. 743

Mathias, P., Gillet, D., & Crowe, R. 1992, A. & A., 257, 681

Pavlovski, K., Harmanec, P. et al. 1997, Astr. Ap. Sup., 125, 75

Peters, G. J. 1991, Rapid Variability of OB-Stars, ed. D. Baade, ESA Conf. Proc. No. 36, p. 171

Peters, G. J. 1994, Pulsation, Rotation, & Mass Loss in Early-Type Stars, ed. L. Balona, H. Henrichs, J. Le Contel (Dordrecht: Kluwer), p 284

Peters, G. J. 1998a, ApJ, 502, L59

Peters, G. J. 1998b, Cyclical Variability of Stellar Winds, eds. L. Kaper & A. W. Fullerton (Springer: Berlin), p. 127

Peters, G. J., & Gies, D. R. 2000, The Be Phenomenon in Early-Type Stars, op. cit., p. 375

Peters, G. J., & Polidan, R. S. 1984, ApJ, 283, 745

Rivinius, T. 1999, priv. communication.

Quirrenbach, A., Bjorkman, K. S. et al. 1998, ApJ, 479, 477

Sareyan, J. P., Gonzalez-Bedolla, S. et al. 1998, A. & A., 332, 155

Shore, S. N., & Brown, D. N. 1990, ApJ, 365, 665

Smith, M. A. 1983, ApJ, 265, 338

Smith, M. A. 1999a, PASP, 111, 722

Smith, M. A. 1999b, PASP, 111, 1472

Smith, M. A. 2000a, The Be Phenomenon in Early-Type Stars, *op cit.*, p. 216

Smith, M. A. 2000b, The Be Phenomenon in Early-Type Stars, *op. cit.*, p. 292

Smith, M. A., Fullerton, A. W., & Percy, J. R. 1987, ApJ, 320, 768

Smith, M. A., & Groote, D. 2001, A. & A., in press

Smith, M. A., & Polidan, R. P. 1993, ApJ, 367, 302

Smith, M. A. & Robinson, R. D. 1999, ApJ, 517, 866

Smith, M. A., Robinson, R. D., & Hatzes, A. P. 1998, ApJ, 507, 945

Smith, M. A., & Groote, D. 2001, A. & A., in press

Stamford, P. A., & Watson, R. D. 1981, Proc. Astr. Soc. Aust., 4, 210

Stefl, S., Baade, D., et al. 1998, A Half Century of Stellar Pulsations, ed. P. Bradley & J. Guzik, ASP Conf. Ser. 135, 348

Stefl, S., Budovicova, A., et al. 2000, The Be Phenomenon in Early-Type Stars, *op. cit.*, p. 240

Thackeray, A. D., 1966, MmRAS, 70, 33

Tubbesing, S., Rivinius, T., & Wolf, B., 2000, The Be Phenomenon in Early-Type Stars, op. cit., p. 232

Vakili, F., Mourard, D., et al. 1998, A. & A., 335, 261

van Kerkwijk, M. H., van Paradijs, J., Zuiderwijk, E. J., Hammerschlag-Hensberge, G.,

Kaper, L., & Sterken, C. 1995, A. & A., 303, 483

This manuscript was prepared with the AAS LaTeX macros v4.0.

Table 1: Summary of Spectrophotometric Characteristics for Be Stars

Group 1	(Pulsation)		
	Sp.	Period (d)	Vsin i
DU Eri	B2V:ne	1.2[1]	340
λ Eri	B2IVne	0.701[2]	310
η Cen	B1Vne	0.642[3]	350
2 Vul	B0.5IV	0.35:[1]	332
EW Lac	B3IVpe	0.722[4]	340
Group 2			
α Eri	B3pe	1.26[5]	220
ψ Per	B5Ve	1.04[6]	369
ω Ori	B3IIIe	1.9[2]	160
PP Car	B4Vne	0.8:[7]	303
28 Cyg	B2.5Ve	0.646[8]	310
ϵ Cap	B3V:p	0.98[1]	293
120 Tau	B1.5IVe	0.5:[1]	271
o And	B6IIIpe	1.58[8]	330
Group 3	(Cloud-like)		
ζ Tau	B4IIIe	0.78[10]	320
60 Cyg	B1Ve	2.48[11]	220
γ Cas	B0.5IVe	1.12:[12]	220

[1]Peters & Gies 2000, [2]Balona et al. 1987, [3]Balona 1999, [4]Floquet et al. 2000, [5]Balona et al. 1987, [6]Peters 1994, [7]this paper, [8]Tubbesing et al. 2000, [9]Sareyan et al. 1998, [10]Kaye

& Gies 1998, [11]Harmanec et al. 1986, [12]Smith et al. 1998.

Figure Captions

Figure 1: The binned ratioed spectrum of two *SWP*-camera echellograms of α Eri (SWP 55889 and 55873) processed through two different spectral extraction algorithms, *NEWSIPS* and *IUESIPS*. The dotted line shows the effect of an assumed 2% error in background level on this ratio. Note its rapid increase below λ1250.

Figure 2: Computed binned absorption spectra of a homogeneous cloud for the variety of temperatures indicated, a column density of 1×10^{23}, and a microturbulence of 20 km s^{-1}. The mean photospheric temperature for these examples is 22,000 K.

Figure 3: **(a)** Ratio of synthesized photospheric spectra over the wavelength range of the *IUE SWP* camera for Kurucz models having log g = 4 and T_{eff} = 26,000 K and 22,000 K. **(b)** Run of temperature with the atmospheric parameter "rhox" for a 22,000 K, log g Kurucz model (dashed line), as altered artificially to mimic a low and high thermal gradient (solid lines). **(c)** The far-ultraviolet ratioed spectrum resulting from the two altered temperature gradient distributions shown in panel **(b)**.

Figure 4: **(a)** UV continuum light curve of Vela X-1, with $\phi = 0.0$ reckoned from eclipse of the neutron star *behind* the B star at HJD 2444279.0466 (van Kerkwijk et al. 1995) for all available high-dispersion *SWP* observations over epochs 1978–93. **(b)** Model and *IUE* spectrum ratio are exhibited as dashed and solid lines, respectively for orbital phases 0.4–0.46 (SWP 01442, 18823, 22324, 32961, 46167, & 49202) divided by observations taken near phase 0.3 (SWP19061-2, 22309 & 46151; see arrow in panel (a)). **(c)** Model and observed spectrum ratio are shown as dashed and solid lines, respectively, for phases 0.5–0.6 (SWP 03510, 03649, 138958, 19012, 25881-2, 32961, 32967, 49086), again divided by observations taken near phase 0.3 (as in panel b). Note the high temperature and column density and low coverage for the best-fit cloud

model. This suggests an hot circumstellar structure which partially obscures the B supergiant primary just after transit of the orbiting X-ray pulsar.

Figure 5: **(a)** The UVC light curve for 88 Her in 1981–1992. **(b)** Spectral ratios of 1986 spectra (SWP 27266, 27672, & 28334) relative to ∼1982 spectra (SWP 14701, 15012, & 16287). **(c)** Comparison of spectra in the λ1910 region. The dashed line represents the spectrum from SWP 31189; solid line from SWP 38786 & 44980. Note that the strengths of the high-excitation Fe III (≈10 eV) lines (asterisked symbols) are highly variable compared to the two Fe III 3.7 eV lines (labeled). The X-symbol denotes pixels excluded because of an instrumental reseau.

Figure 6: **(a)** The UVC light curve for ζ Tau. Observations indicated by arrows are SWP 42644, 42650, 42658, & 42664. **(b)** Solid line shows spectral ratio taken from the binned fluxes of SWP 42644 & 42658 divided by SWP 42650 & 42664 (arrows in **a**); dashed line is from a *CIRCUS* model with the indicated parameters. **(c)** Comparison of spectra in the λ1860 (Al III line) region. The top line represents the mean spectrum from all 1991 observations. The bottom line is the r.m.s. spectrum, with line excitations indicated in eV.

Figure 7: **(a)** The UVC light curve for 60 Cyg in late July, 1995. **(b)** Solid line shows spectral ratio for 60 Cyg taken from the binned fluxes of SWP 55536 divided by SWP 55608 (arrows in **a**); dashed line is from a *CIRCUS* model with the indicated parameters. **(c)** Comparison of the same two spectra in the λ1855-63 (Al III line) region. The bottom line is the r.m.s. spectrum, with line excitations indicated in eV. This panel shows that even that variations of low-excitation lines are visible even in this broad-lined star.

Figure 8: Montage of ratioed spectra of *known* β Cep stars with primarily radially pulsating modes and one large-amplitude nonradially pulsating B star, ϵ Per. Offsets

in a few cases are noted for clarity. The dot-dashed line depicts the simulated ratioed spectrum resulting from division of spectra with different T(ρ x) distributions, as shown in Fig.3c. The dashed line represents the ratioed spectrum of the large-amplitude, nonradially pulsating star, ϵ Per. These ratioed spectra exhibit pulsation signatures discussed in the text which are used in Table 1 to differentiate between Groups 1 & 2. The ratioed spectra shown (maximum-flux phase divided by minimum-flux) are given by *SWP* sequence number as follows: BW Vul, 05590-1, 05597-8 vs. 05594-5; ν Eri, 04355 vs. 04351-2; 12 Lac, 55699 vs. 55710; α Lup, 04572-4 vs. 04564-6; δ Cet, 04487-8 vs. 04490-1; β Cep, 04596-7 vs. 04598-9; and ϵ Per, 56521-2, 56577-8 vs. 56524-6.

Figure 9: *a* Montage of ratioed spectra for *presumed* pulsating stars. The upper two spectra have the $\lambda\lambda$1240–1380 "window" signature of strong (indicated by bar with downward errors and spike at λ1300) and a plateau at $\lambda\lambda$1400–1540 (bar with upward arrows), as expected from strong NRP or radial pulsations, according to Fig. 8. *b* Display of ratioed spectra with a nearly a monotonic form with wavelength, as expected from simple models of small-amplitude NRP (Group 2). *IUE* sequence numbers for ratioed spectra for bright and faint-star phases for the two panels are as follows: η Cen, 41218, 41230, 41254, 41257 vs. 41213, 41234, 41237, 41248, 41260; λ Eri, 32228, 32246, 32262 vs. 32238, 32254; EW Lac, 48556, 48558, 48560 vs. 48546, 48548, 48564, 48566, 48568; ω Ori, 56751–55 vs. 56739–43, DU Eri, 55888 vs. 55882, 55892; *o* And, 31479, 31481 vs. 31489, 31491; ϵ Cap, 34367, 34369, 34386, 34388, 34390, 34392 vs. 34378, 34380; and 28 Cyg, 37132, 37134 vs. 37100, 37102.

Fig. 1.— msfig1

Fig. 2.— msfig2

Fig. 3.— msfig3

Fig. 4.— msfig4

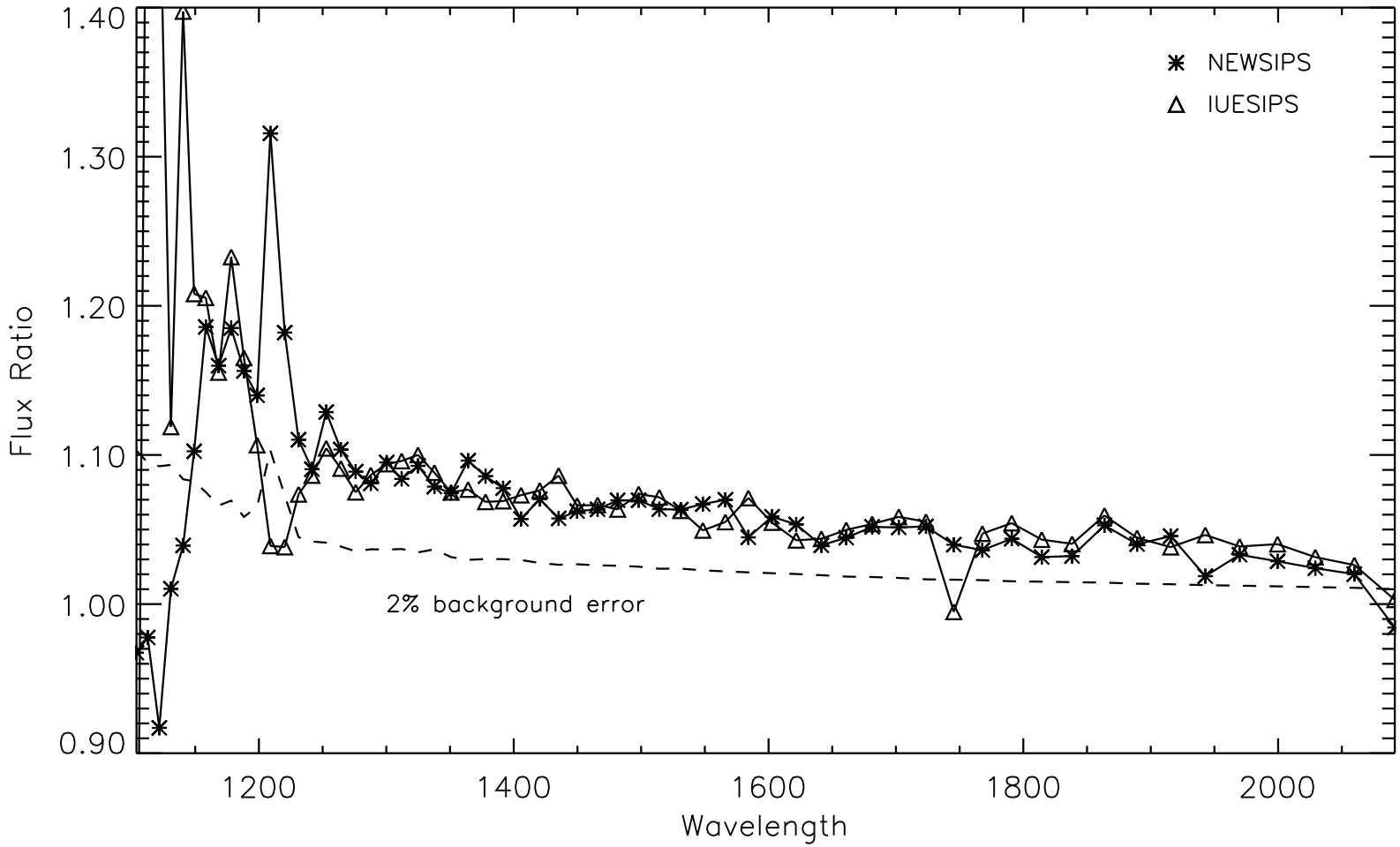
Fig. 5.— msfig5

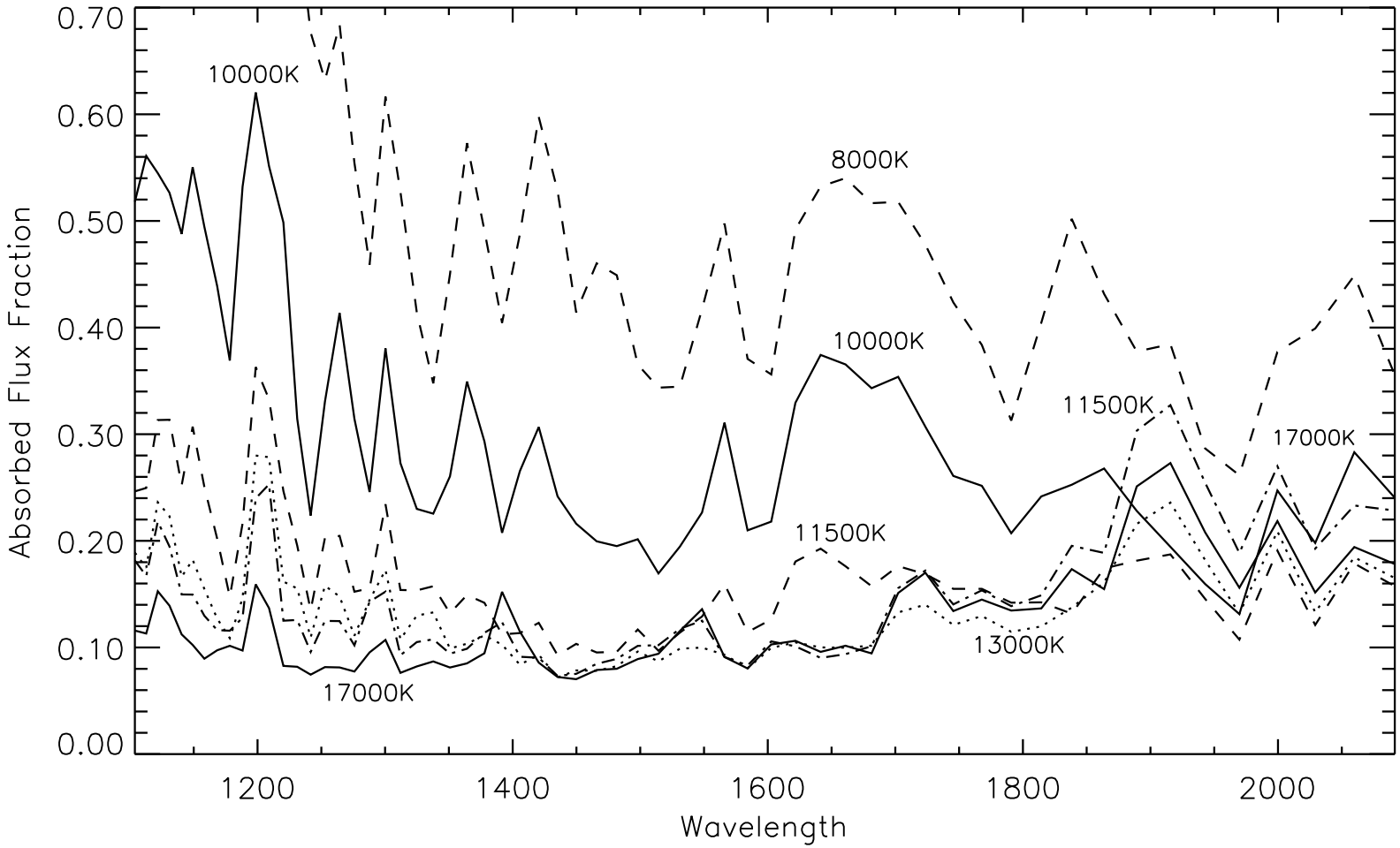
Fig. 6.— msfig6

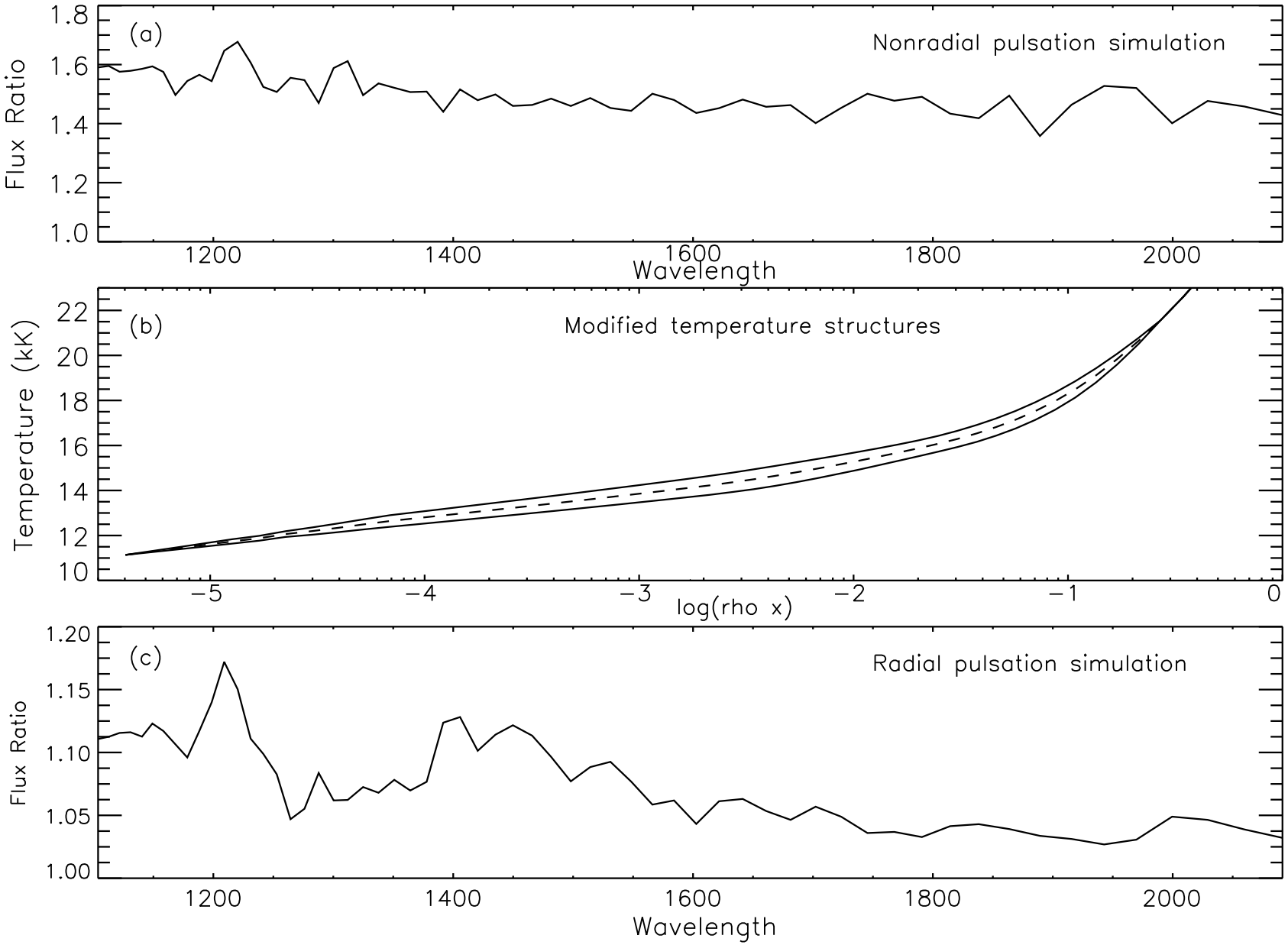
Fig. 7.— msfig7

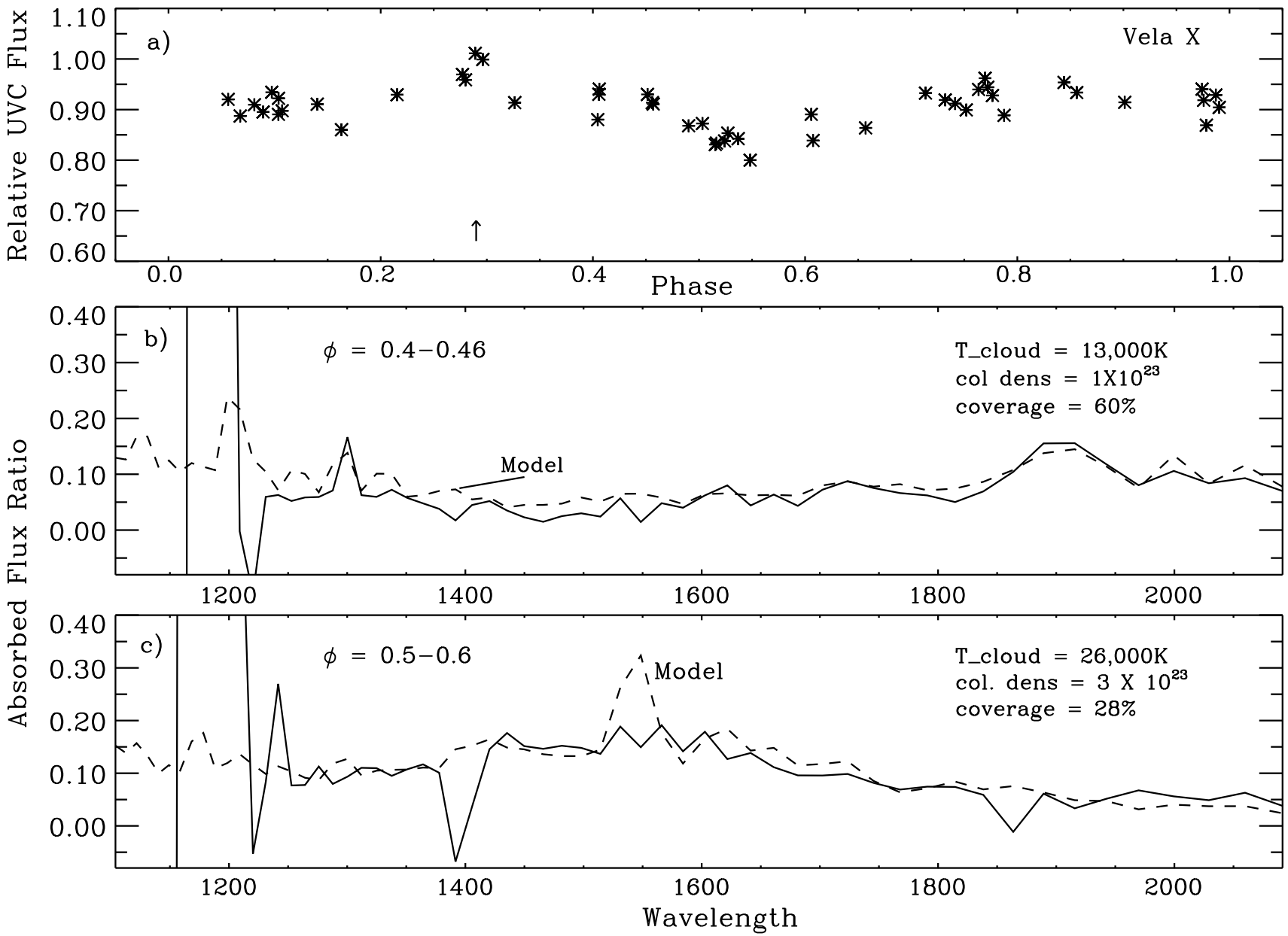
Fig. 8.— msfig8

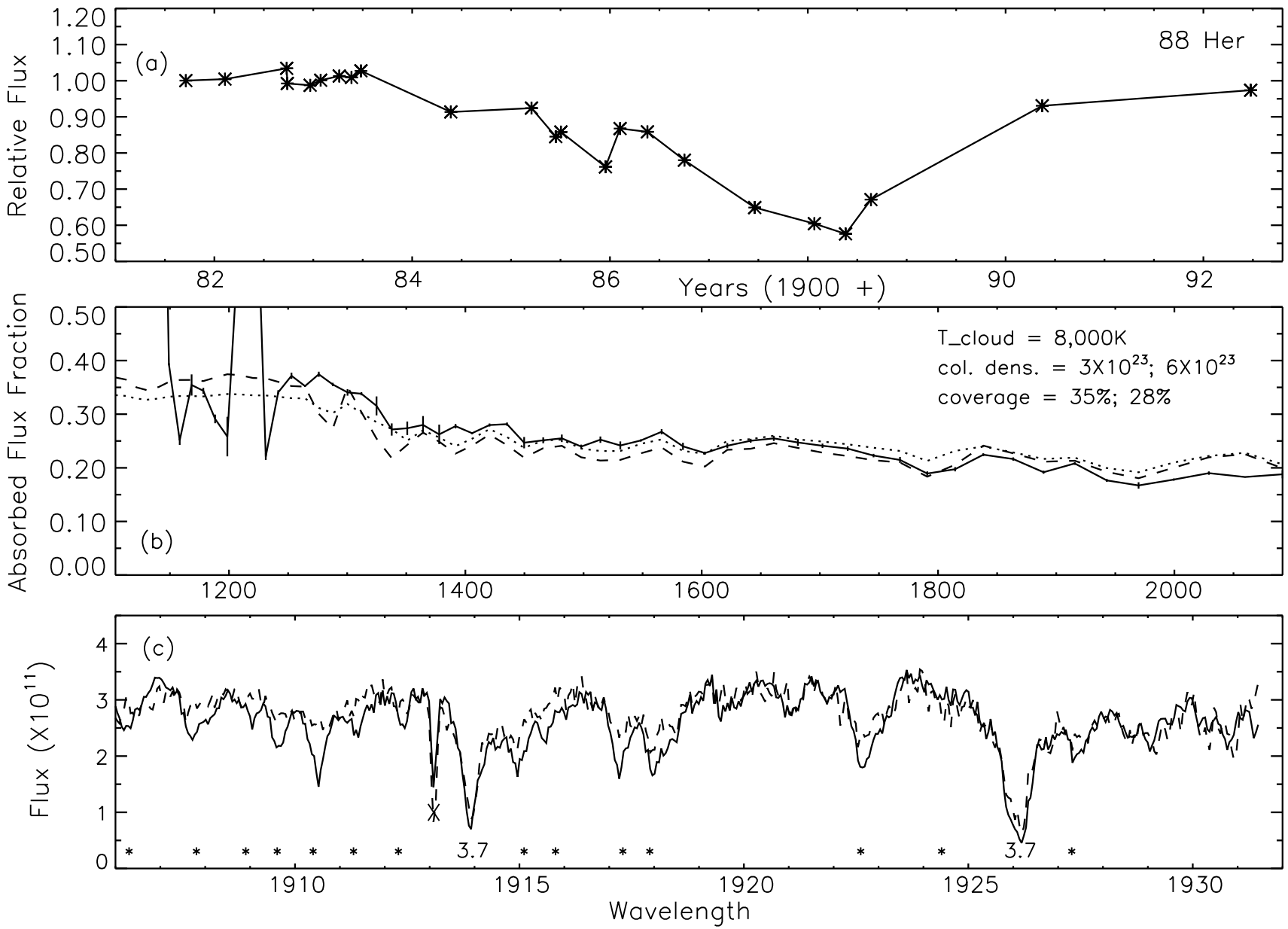
Fig. 9.— msfig9

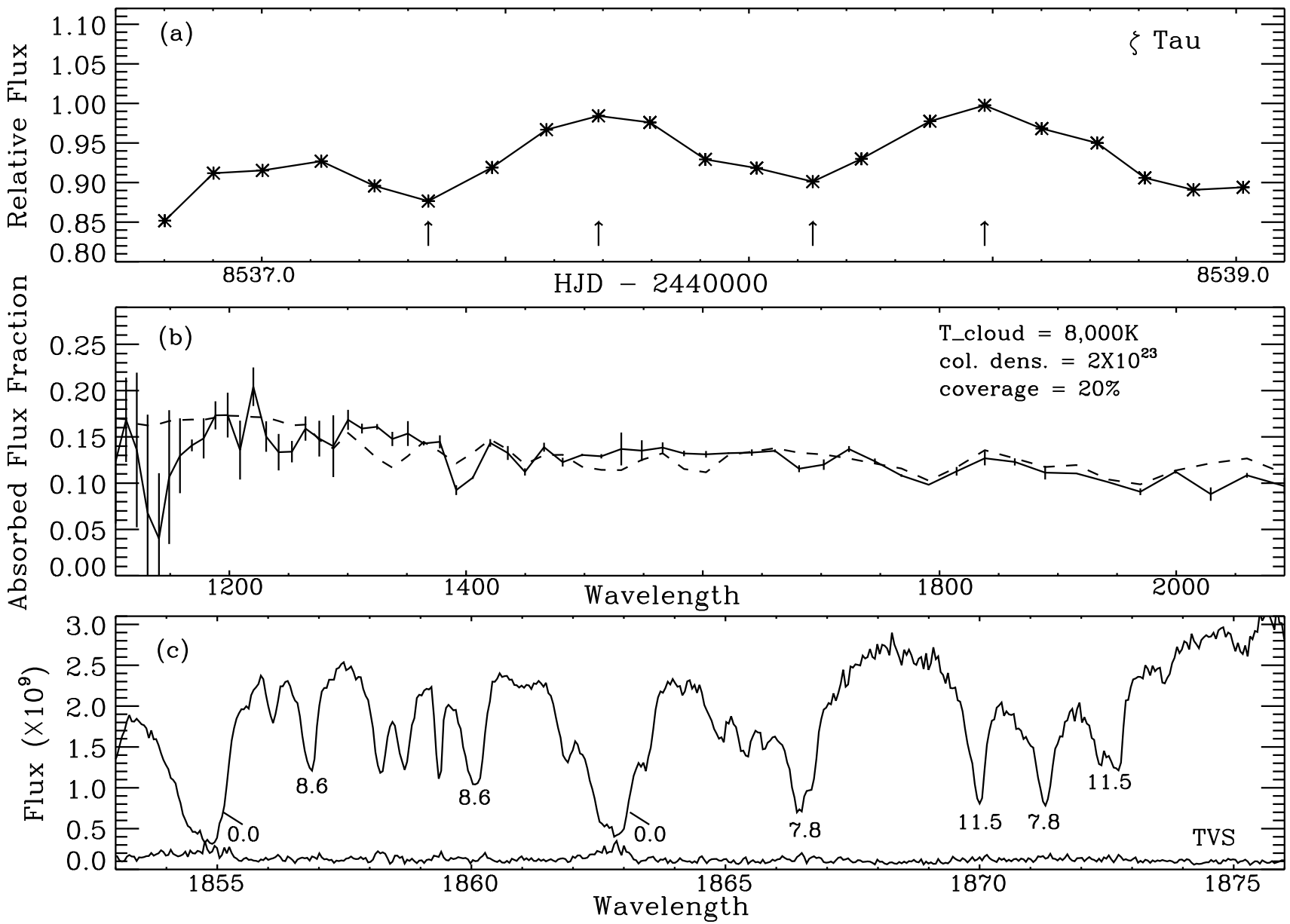

1.40
1.30
1.20
1.10
1.00
0.90
Flux Ratio
1200
1400
1600
1800
2000
Wavelength
NEWSIPS
IUESIPS
2% background error

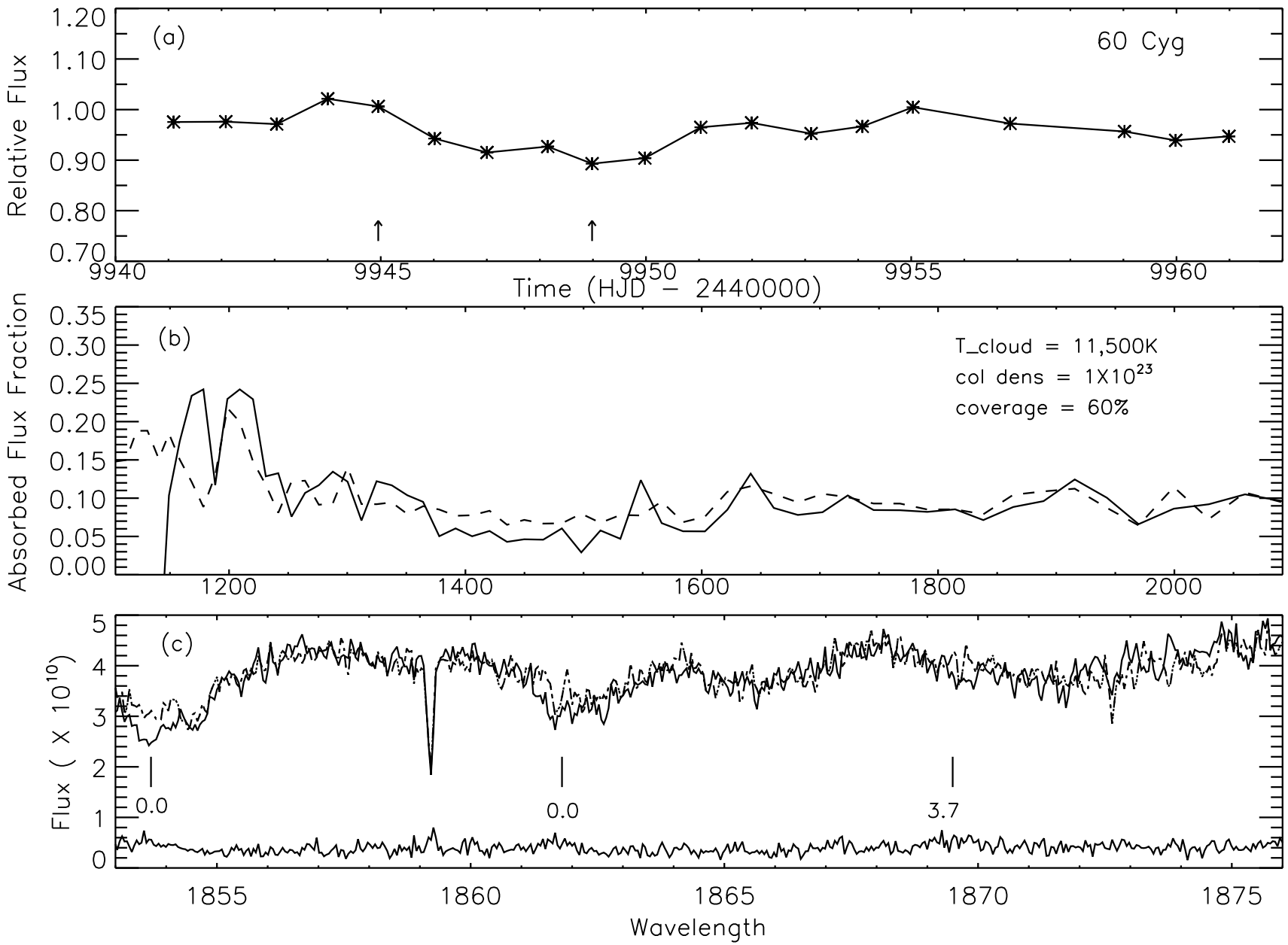

0.70
0.60
0.50
0.40
0.30
0.20
0.10
0.00
Absorbed Flux Fraction
1200
1400
1600
1800
2000
Wavelength
10000K
8000K
10000K
11500K
17000K
11500K
13000K
17000K

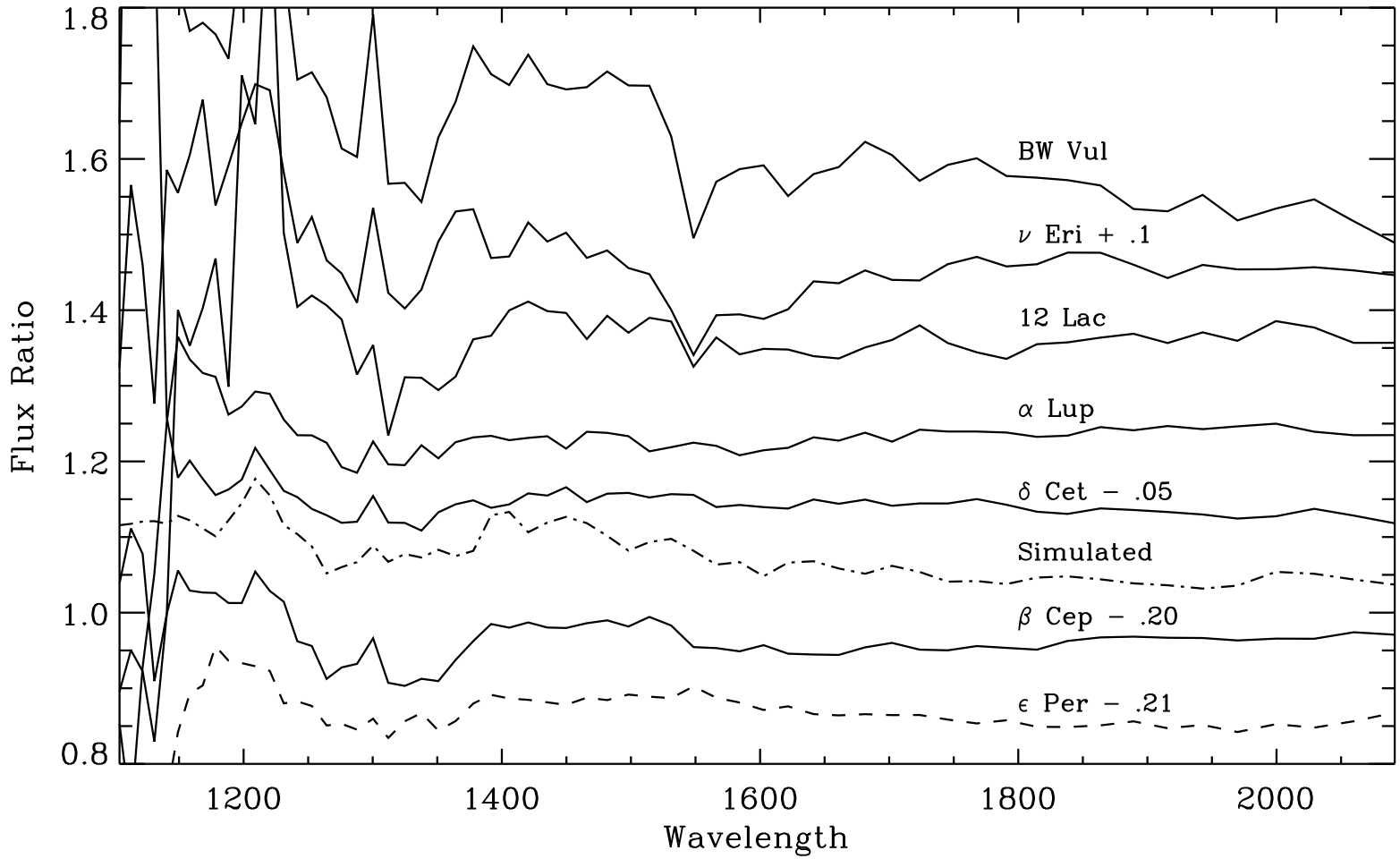

(a)
Nonradial pulsation simulation
Flux Ratio
1.8
1.6
1.4
1.2
1.0
1200
1400
1600
1800
2000
Wavelength
(b)
Modified temperature structures
Temperature (kK)
22
20
18
16
14
12
10
−5
−4
−3
−2
−1
0
log(rho x)
(c)
Radial pulsation simulation
Flux Ratio
1.20
1.15
1.10
1.05
1.00
1200
1400
1600
1800
2000
Wavelength

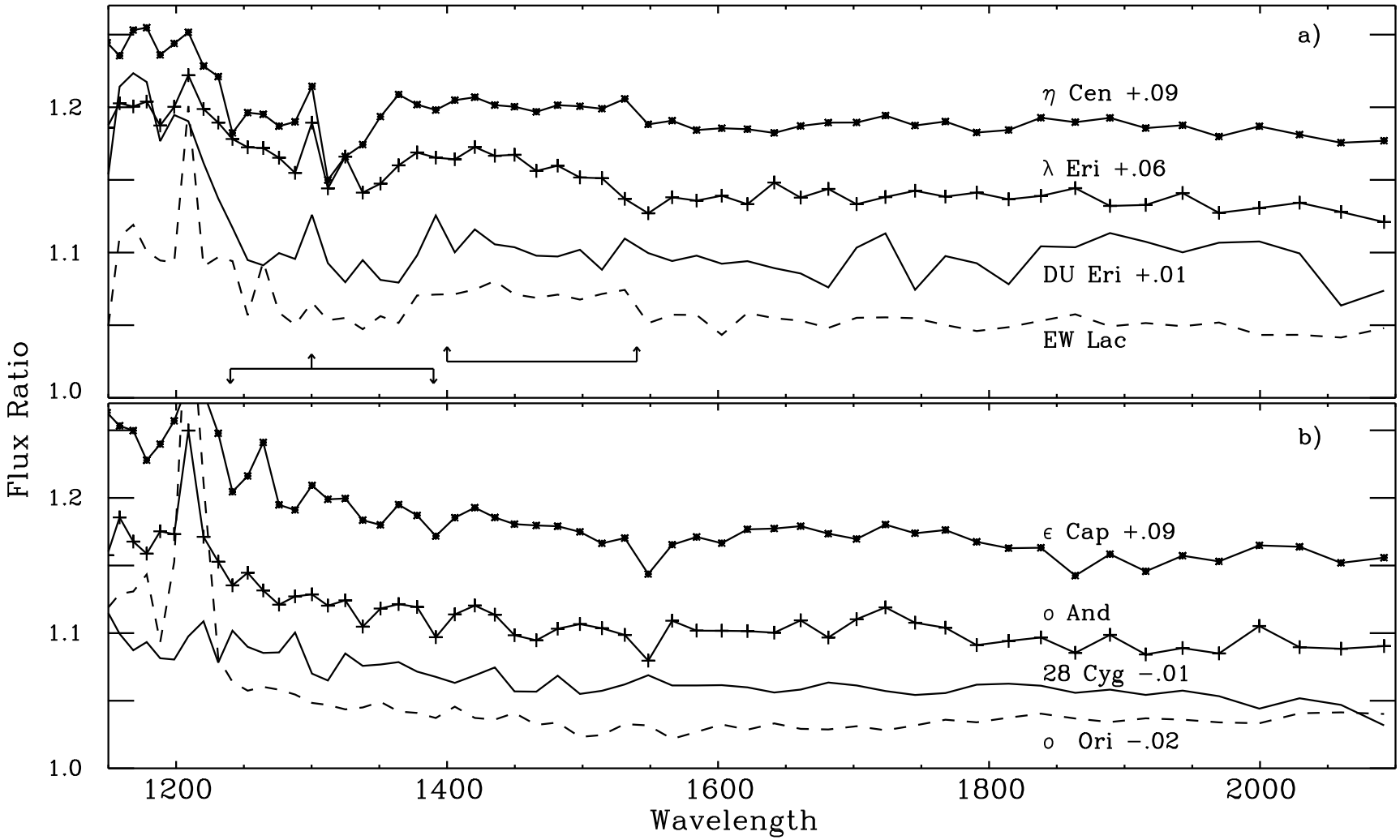

a)
Vela X
Relative UVC Flux
1.10
1.00
0.90
0.80
0.70
0.60
0.0
0.2
0.4
0.6
0.8
1.0
Phase
b)
ϕ = 0.4−0.46
T_cloud = 13,000K
col dens = 1X10^{23}
coverage = 60%
Model
Absorbed Flux Ratio
0.40
0.30
0.20
0.10
0.00
1200
1400
1600
1800
2000
c)
ϕ = 0.5−0.6
Model
T_cloud = 26,000K
col. dens = 3 X 10^{23}
coverage = 28%
Wavelength


(a)
88 Her
Relative Flux
1.20
1.10
1.00
0.90
0.80
0.70
0.60
0.50
82
84
86
90
92
Years (1900 +)
(b)
T_cloud = 8,000K
col. dens. = 3X10^23; 6X10^23
coverage = 35%; 28%
Absorbed Flux Fraction
0.50
0.40
0.30
0.20
0.10
0.00
1200
1400
1600
1800
2000
(c)
Flux (X10^11)
4
3
2
1
0
3.7
3.7
1910
1915
1920
1925
1930
Wavelength


(a)
ζ Tau
Relative Flux
1.10
1.05
1.00
0.95
0.90
0.85
0.80
8537.0
HJD − 2440000
8539.0
(b)
T_cloud = 8,000K
col. dens. = 2X10^23
coverage = 20%
Absorbed Flux Fraction
0.25
0.20
0.15
0.10
0.05
0.00
1200
1400
Wavelength
1800
2000
(c)
Flux (X10^9)
3.0
2.5
2.0
1.5
1.0
0.5
0.0
8.6
8.6
0.0
0.0
7.8
11.5
7.8
11.5
TVS
1855
1860
1865
1870
1875
Wavelength


(a)
60 Cyg
Relative Flux
1.20
1.10
1.00
0.90
0.80
0.70
9940
9945
9950
9955
9960
Time (HJD − 2440000)
(b)
T_cloud = 11,500K
col dens = 1X10^23
coverage = 60%
Absorbed Flux Fraction
0.35
0.30
0.25
0.20
0.15
0.10
0.05
0.00
1200
1400
1600
1800
2000
(c)
Flux (X 10^10)
5
4
3
2
1
0
0.0
0.0
3.7
1855
1860
1865
1870
1875
Wavelength


1.8
1.6
1.4
1.2
1.0
0.8
Flux Ratio
1200
1400
1600
1800
2000
Wavelength
BW Vul
ν Eri + .1
12 Lac
α Lup
δ Cet − .05
Simulated
β Cep − .20
ε Per − .21


a)
η Cen +.09
λ Eri +.06
DU Eri +.01
EW Lac
b)
ε Cap +.09
o And
28 Cyg −.01
o Ori −.02
Flux Ratio
1.0
1.1
1.2
1200
1400
1600
1800
2000
Wavelength